A Family of Vortices to Study Axisymmetric Vortex Breakdown and Reconnection

Larry A. Young[1]
NASA Ames Research Center, Moffett Field, CA, 94035-1000

A new analytic model describing a family of vortices has been developed to study some of the axisymmetric vortex breakdown and reconnection fluid dynamic processes underlying body-vortex interactions that are frequently manifested in rotorcraft and propeller-driven fixed-wing aircraft wakes. The family of vortices incorporates a wide range of prescribed initial vorticity distributions -- including single or dual-core vorticity distributions. The result is analytical solutions for the vorticity and velocities for each member of the family of vortices. This model is of sufficient generality to further illustrate the dependence of vortex reconnection and breakdown on initial vorticity distribution as was suggested by earlier analytical work. This family of vortices, though laminar in nature, is anticipated to provide valuable insight into the vortical evolution of large-scale rotor and propeller wakes.

Nomenclature

r	Radial coordinate, origin at filament axis, m
$r^{\bullet}$	Nondimensional radial coordinate, $r^{\bullet} = r/r_{c0}$
r_o	Spherical finite-volume source terms' "effective" initial radius, m
r_{c0}	"Finite core" vortex filament core size radius (at time equal to zero), m
Re	Vortex Reynolds number, $\mathrm{Re} = \gamma/\nu$
t	Time, sec
$t^{\bullet}$	Nondimensional time parameter, $t^{\bullet} = \nu t/r_{c0}^2$
$\mathbf{V}$	Velocity vector, cylindrical coordinates, $\mathbf{V} = \begin{bmatrix} v_r & v_\theta & v_z \end{bmatrix}$, m/sec
V_p	Finite core vortex axial flow "wave front" propagation velocity, m/sec
z	Axial (along vortex filament axis) coordinate, origin at intersection of filament segments' plane of symmetry and filament axis, m
$z^{\bullet}$	Nondimensional axial coordinate, $z^{\bullet} = z/r_{c0}$
z_w	Wave front boundary, m
γ	Vortex filament initial circulation strength, m^2/sec
Γ	Vortex circulation, m^2/sec
ν	Kinematic viscosity, m^2/sec
θ	Angular coordinate, radians
$\boldsymbol{\omega}$	Vorticity vector, $\boldsymbol{\omega} = \begin{bmatrix} \omega_r & \omega_\theta & \omega_z \end{bmatrix}$, 1/sec

[1] Aerospace Engineer, Aeromechanics Branch, Flight Vehicle Research and Technology Division, Mail Stop 243-12, AIAA Associate Fellow.

I. Introduction

VORTEX filament "cutting" by solid bodies occurs in a number of real world examples for rotary-wing aircraft. These examples include blade vortex interactions where vortices shed from one rotor blade come in close proximity with another blade, trailed tip vortex interactions with a helicopter airframe/tailboom in hover and low-speed flight, or, alternatively, proprotor vortex interactions with wing surfaces for tiltrotor aircraft in airplane-mode. There are two schools of thought regarding when such vortices perpendicularly intersect the vehicle airframe. The first school of thought envisions the vortex "wrapping" around the solid body/surface and reconnects near-seamlessly after passing around the body. The second school, as discussed herein this paper, anticipates that the vortex is "cut" or "broken" such that the vortex circulation between "breakpoints" is, for a time, greatly diminished. There is experimental evidence supporting the proposition that vortex filaments can be "cut" or "broken" during perpendicular body-vortex interactions. References 1-3, for example, provide qualitative discussion regarding vortex filament "cutting" as manifested in the form of blade vortex interactions. References 4-7 provide similar qualitative discussion of vortex fuselage/airframe/wing interactions.

Very little work to date has been performed, though, examining the post-cut/collision unsteady fluid dynamics of perpendicular, or orthogonal, vortex/solid body interactions. Most work has either concentrated on the vortex/body interaction process itself (see Ref. 8) or, alternatively, has looked at vortex-on-vortex interactions. A related topic is the study of ring vortices during vortex/vortex and vortex/body interactions; see Ref. 9, for example. Though flow visualization techniques are of sufficient maturity so as to examine in detail the rotary-wing/airframe vortex filament collision process - see, in particular, Refs. 4, 5, and 7 -- it's clear that current rotor wake theoretical analysis is as yet inadequate to accurately model the vortex breakdown or reconnection processes subsequent to body/vortex interaction. This work summarizes an expanded analysis approach, building on the earlier work of Refs. 10-11, to study these vortical flow processes, i.e. post-filament-cutting during body/vortex interaction.

A class of flow problem will be studied that not only encompasses the "moving boundary" class of problems (including the classic Lamb-Oseen vortex) but the vortex reconnection problem as well. Integral to this class of flow problem is the assumption that the axial and radial velocity components, v_z and v_r, are not merely equal to zero (as in the case of the Lamb-Oseen vortex) but the radial velocity is instead proportional to the tangential velocity gradient, e.g.

$$v_r \propto \frac{\partial v_\theta}{\partial z} \tag{1}$$

Or

$$v_r = \ell \frac{\partial v_\theta}{\partial z} \tag{2}$$

The length scale factor, ℓ, is a constant -- at least within discrete spatial regions -- that transforms the proportional relationship of Eq. 1 to the equivalence relationship of Eq. 2. The constant ℓ has the unit of length, hence it being called a "length scale factor." This is discussed in detail in Refs. 10-11. Correspondingly, a second proportional relationship, based on flow continuity, can be defined for the axial velocity.

$$v_z \propto -\left(\frac{\partial v_\theta}{\partial r} + \frac{v_\theta}{r} \right) \tag{3}$$

Or

$$v_z = -\ell \left(\frac{\partial v_\theta}{\partial r} + \frac{v_\theta}{r} \right) \tag{4}$$

This, in turn, dictates that the vorticity can be related to the velocity components.

$$v_z = -\ell\omega_z$$

$$v_r = -\ell\omega_r \tag{5a-b}$$

Applying a length-scale factor causes the convective acceleration terms to cancel out the vortex stretching terms and thereby reducing the Helmholtz equations to the unsteady heat conduction equation (Eq. 6) for the axial vorticity.

$$\frac{D\boldsymbol{\omega}}{Dt} = (\boldsymbol{\omega}\cdot\nabla)\mathbf{V} + \nu\nabla^2\boldsymbol{\omega}$$

$$\downarrow$$

$$\frac{\partial\omega_z}{\partial t} = \nu\left\{\frac{\partial^2\omega_z}{\partial r^2} + \frac{1}{r}\frac{\partial\omega_z}{\partial r} + \frac{\partial^2\omega_z}{\partial z^2}\right\} \tag{6}$$

There is a large body of work related to the analytical solution of the heat conduction equation, including the use of unsteady finite-volume source modeling, that enabled the derivation of (albeit laminar) solutions for the vortex reconnection problem. It is important to note, though, that the length-scale factor methodology, for the vortex reconnection results, yields solutions that are only approximate in nature. Though the Helmholtz equation for axial vorticity is exactly satisfied, for the cases where $\omega_r \neq 0$ and $\omega_\theta \neq 0$, i.e. non-columnar flow, the corresponding equations for the radial and azimuthal vorticity are satisfied only approximately. This will be discussed further later in the paper.

Analytical descriptions of vortex filament reconnection and breakdown phenomena -- subsequent to "cutting" or, rather, collision with a solid body -- were first derived in Refs. 10 and 11 for four different initial vorticity distributions: instantaneous (line source), uniform, parabolic, and dual-core (inner core with negative vorticity) finite-core vortex models. In particular the dual-core model exhibited interesting vortical flow characteristics not only with regards to vortex filament reconnection but it also manifested flow behavior analogous to that observed and (numerically) predicted for vortex breakdown. (On the other hand, the dual-core model also had many limitations including providing unrealistic, nonphysical predictions at very small values of time.) Though the earlier solutions provided considerable insight into vortex filament reconnection and breakdown, the dependence of the analytical solutions to a few specific instances of initial axial vorticity distribution provided an incomplete understanding of this vortical flow problem. A more general approach was ideally needed. Therefore, a new family of vortices has been derived in this paper that allows a more general treatment of the vortex filament breakdown and reconnection unsteady flow problem. The analytical treatment, detailed in the Appendix, is, in large part, an extension of the earlier work of Refs. 10 and 11.

II. Overview of Analytical Work

An extended length-scale-factor methodology is introduced so as to examine a more general set of initial vorticity distributions for the vortex reconnection problem. In particular, this methodology enables a unique superposition of vortex sources terms to define this general set of initial vorticity distributions. This extended methodology can now accommodate multiple (greater than two) breakpoints as well as discrete/finite distributions of vorticity in addition to the earlier studied semi-infinite distributions. Given this extended methodology, the vorticity and velocity distributions during vortex reconnection can now be described as follows

$$\omega_z = \sum_{i=1}^{N} \Delta\omega_z\left(\gamma_i, r_{o_i}, a_i, b_i, r, z, t\right)$$

$$v_z = \sum_{i=1}^{N} f\left(N, i, \gamma_i, r_{o_i}, a_i, b_i, r, z, t\right)$$

Where

$$f\left(N, i, \gamma_i, r_{o_i}, a_i, b_i, r, z, t\right) = \ell\left(N, i, z\right)\Delta\omega_z\left(\gamma_i, r_{o_i}, a_i, b_i, r, z, t\right)$$

(7a-c)

Where $\ell(\ldots)$ is the length scale factor, which is defined in terms of a "local" definition of symmetrical or nonsymmetrical flow. The incremental vorticity function $\Delta\omega_z(\ldots)$ is defined in the Appendix. Infinite vortex segments are a special case wherein $\ell(\ldots) = 0$ and, therefore, $f(\ldots) = 0$.

Where, in the above, the following cases apply: $N = 2$ for one isolated "free" breakpoint and $N = 4$ for two breakpoints in close proximity to each other. The following conventions are employed in this paper. First, as to ordering conventions for the above arrays: 1. no vortex filament segment can cross-over $z = 0$, i.e. $a_i b_i \geq 0$, with the exception of infinite vortex filaments; 2. odd indices are assigned for $a_i \geq 0$ and, correspondingly, $b_i \geq 0$, and even indices for $a_i < 0$ and, correspondingly, $b_i < 0$; 3. indices are assigned in order of increasing $|b_i|$; 4. semi-infinite, where $|b_i| = \infty^-$, or infinite, $a_i = -\infty^+$ and $b_i = \infty^-$, segments are the last entries in the array; 5. infinite vortex filaments should ideally, though not as an absolute rule, be replaced by two semi-infinite vortex filaments segments; 6. vortex segments can partially or fully overlay each other (this implied superposition is fundamental to defining the general family of vortices studied in this paper). The primary rationale for this particular ordering convention is the implicit ease in truncating, as needed from a numerical efficiency perspective, vortex filament segments that are far removed from $z = 0$. Additionally, the convention for defining the nominal initial vortex core radius is as follows: r_{c0} is defined on the basis of the "upstream" far-field vortex geometry and initial conditions, i.e. r_{c0} is defined at the limit where $z \to \infty$. Therefore, it is possible to, even at $t \to 0$, to prescribe different vortex core size distributions, albeit initially discrete in nature, for the complete ensemble of vortex segments defining the complete vortex filament. To emphasize this point further, it is possible to have different core sizes between the upstream, $z \geq 0$, and downstream, $z < 0$, vortex filaments; nonetheless, the nominal reference value of r_{c0} is the upstream far-field limit, i.e. r_{c0A}, by convention. Therefore, the key flow parameters are nondimensionalized, in part, by the upstream far-field vortex core radius, r_{c0A}.

For $N = 4$, the two-breakpoint case, the following arrays are defined

$$\gamma = \begin{bmatrix} \chi_A\gamma_A \\ \chi_B\gamma_B \\ \gamma_A \\ \gamma_B \end{bmatrix} \qquad r_o = \begin{bmatrix} \eta_A r_{oA} \\ \eta_B r_{oB} \\ r_{oA} \\ r_{oB} \end{bmatrix} \qquad a = \begin{bmatrix} s \\ -s - \ell_B \\ s \\ -\infty^+ \end{bmatrix} \qquad b = \begin{bmatrix} s + \ell_A \\ -s \\ \infty^- \\ -s \end{bmatrix} \tag{8a-d}$$

And where, for $N = 2$, the isolated "free" case, the arrays are

$$\gamma = \begin{bmatrix} \chi_A\gamma_A \\ \gamma_A \end{bmatrix} \qquad r_o = \begin{bmatrix} \eta_A r_{oA} \\ r_{oA} \end{bmatrix} \qquad a = \begin{bmatrix} 0 \\ 0 \end{bmatrix} \qquad b = \begin{bmatrix} \ell_A \\ \infty^- \end{bmatrix} \tag{9a-d}$$

Finally, for columnar vortices, in general, $N = 2$ and the arrays are

$$\gamma = \begin{bmatrix} \chi_A \gamma_A \\ \gamma_A \end{bmatrix} \qquad r_o = \begin{bmatrix} \eta_A r_{oA} \\ r_{oA} \end{bmatrix} \qquad a = \begin{bmatrix} -\infty^+ \\ -\infty^+ \end{bmatrix} \qquad b = \begin{bmatrix} \infty^- \\ \infty^- \end{bmatrix} \tag{10a-d}$$

However, for the special case of parabolic finite core vortices (where $\chi_A = 0$) then the arrays are

$$\gamma = \begin{bmatrix} \gamma_A \\ \gamma_A \end{bmatrix} \qquad r_o = \begin{bmatrix} r_{oA} \\ r_{oA} \end{bmatrix} \qquad a = \begin{bmatrix} 0 \\ -\infty^+ \end{bmatrix} \qquad b = \begin{bmatrix} \infty^- \\ 0 \end{bmatrix} \tag{11a-d}$$

In all cases the length-scale-factor function, $\ell(\ldots)$, for multiple breakpoints, is given by

$$\ell(N,i,z) = r_{c0A} \cdot u(z_w - z) \qquad \text{For } N = 1$$

$$\ell(N,i,z) \equiv r_{c0A} \cdot signum(a_i) u(z_w - signum(a_i) z) \qquad \text{If } N \geq 2 \text{ and } |b_i| = \infty^- \text{ or } |a_i| = \infty^+$$

$$\ell(N,i,z) \equiv r_{c0A} \cdot signum\left(\frac{1}{2}(b_i + a_i) - z\right) q(i,z)$$

$$\begin{aligned} q(i,z) \equiv\ & u(a_i) u\left(z_w - a_i - \frac{1}{2}(b_i - a_i)\right) u(b_i - z) \\ & + u(-a_i) u\left(z_w + b_i - \frac{1}{2}(b_i - a_i)\right) u(z - a_i) \\ & + u(a_i) u\left(\frac{1}{2}(b_i - a_i) - z_w + a_i\right) \left\{ u(z_w - z) + u(z - b_i + z_w - a_i) u(b_i - z) \right\} \\ & + u(-a_i) u\left(\frac{1}{2}(b_i - a_i) - z_w - b_i\right) \left\{ u(z + z_w) + u(z - a_i) u(z_w + b_i + a_i - z) \right\} \end{aligned}$$

$$\text{If } N \geq 2 \text{ and } |a_i| \leq |b_i| << \infty^-$$

(12a-d)

The above length-scale factors are based in part on the wave front boundary, z_w, which is a function of time. The absolute displacement distance of a given wave front boundary from an individual breakpoint, or finite span of vorticity endpoint, is given by $z_w \approx |C| + \left|\gamma_i / \pi r_{c0_i}\right| t$, where if $a_i \geq 0$ then $C = a_i$ otherwise $C = b_i$. Note that multiple breakpoints result in multiple wave front boundaries. Refer to the Appendix for more details. The Heaviside unit step function, $u(x)$, is defined by $u(x) = 1$ for $x \geq 0$ and $u(x) = 0$ for $x < 0$. The $signum(x)$ function is defined as $signum(x) = 1$ for $x = 0$ and $signum(x) = x/|x|$ for all other values of x.

In many of the cases studied, spanwise symmetry about the breakpoints has been preserved. Therefore many of the primary vortex filament properties such as circulation strength, source and core radius are equal – i.e. $\gamma_A = \gamma_B$, $r_{oA} = r_{oB} = r_o$, and $r_{c0A} = r_{c0B} = r_{c0}$. The vortex segment span lengths can be finite or infinite, equal or non-equal in length, i.e. $\ell_A \leq \infty^-$ and $\ell_B \leq \infty^-$; for most of the work presented in this paper, $\ell_A = \ell_B$ and $|s + \ell_A| = |-s - \ell_B| \leq \infty^-$. Spanwise symmetry is not necessarily required in the analysis, as will be seen for a few cases. Additionally, the analysis can readily account for multiple breakpoints for various (discrete) initial axial vorticity distributions, as seen in Eq. 12a-d.

Similar expressions as that defined for the axial vorticity and velocity, Eq. 7a-c, can readily be defined for the radial and tangential vorticity and velocity components, as in Eq. 13a-f, and are based on the principle of superposition as the axial vorticity solution is satisfied by the classic heat conduction equation and the remaining vorticity and velocity terms are derived on the basis of the vorticity component definitions and the divergence relationship – for more details refer to Refs. 10 and 11. But, to reiterate, the overall solution is approximate in nature for all but columnar vortex predictions. Derivation of the individual incremental vorticity and velocity expressions, i.e. $\Delta\omega_z(\ldots)$, $\Delta v_\theta(\ldots)$, $\Delta\omega_r(\ldots)$, etc., is summarized in the Appendix.

$$v_\theta = \sum_{i=1}^{N} \Delta v_\theta\left(\gamma_i, r_{o_i}, a_i, b_i, r, z, t\right)$$

$$\omega_r = \sum_{i=1}^{N} \Delta\omega_r\left(\gamma_i, r_{o_i}, a_i, b_i, r, z, t\right)$$

$$v_r = \sum_{i=1}^{N} g\left(N, i, \gamma_i, r_{o_i}, a_i, b_i, r, z, t\right)$$

$$\omega_\theta = \sum_{i=1}^{N} \Delta\omega_\theta\left(N, i, \gamma_i, r_{o_i}, a_i, b_i, r, z, t\right)$$

Where

$$g\left(N, i, \gamma_i, r_{o_i}, a_i, b_i, r, z, t\right) = \ell\left(N, i, z\right)\Delta\omega_r\left(\gamma_i, r_{o_i}, a_i, b_i, r, z, t\right)$$

And

$$\Delta\omega_\theta\left(N, i, \gamma_i, r_{o_i}, a_i, b_i, r, z, t\right) = \ell\left(N, i, z\right)h\left(\gamma_i, r_{o_i}, a_i, b_i, r, z, t\right)$$

(13a-f)

The interdependence of the finite-volume source radii, r_{oA} and r_{oB}, and that of the overall vortex filament core radii, r_{c0}, r_{c0A}, etc., is a particularly crucial part of the analysis, an expression for which is derived in the Appendix and summarized below. (Spanwise symmetrical flow is assumed unless otherwise specified; therefore, for most cases studied $r_{oB} = r_{oA}$.)

$$r_{oA} \approx \left(1 + 0.075u\left(1 + \chi_A\right)\left(1 + \chi_A\right)^3\right)r_{c0A}$$

For $-1 \le \chi_A < 0.4$

Or

$$\left(1 + \chi_A\right)r_{oA}^3 - \sqrt{\left(r_{oA}^2 - r_{c0A}^2\right)^3} - 3r_{c0A}^2\sqrt{r_{oA}^2 - r_{c0A}^2} = 0$$

(14a-b)

III. Discussion of an Illustrative Set of Results

It is beyond the scope of this paper to present more than a small fraction of the wide range of initial vorticity distributions – as well as discrete spanwise vortex filament geometries – which can be predicted by the analysis presented in this paper. However, a select number of cases (representative examples being shown in Fig. 1) will be presented that focus on examining the question of the existence and underlying causative factors of the vortex breakdown phenomena that can, but not always, manifest itself during vortex reconnection. But first, recognizing the exactness of the derived analytical solution for columnar vortices, the results for a few of the columnar vortices described by the analysis is next presented.

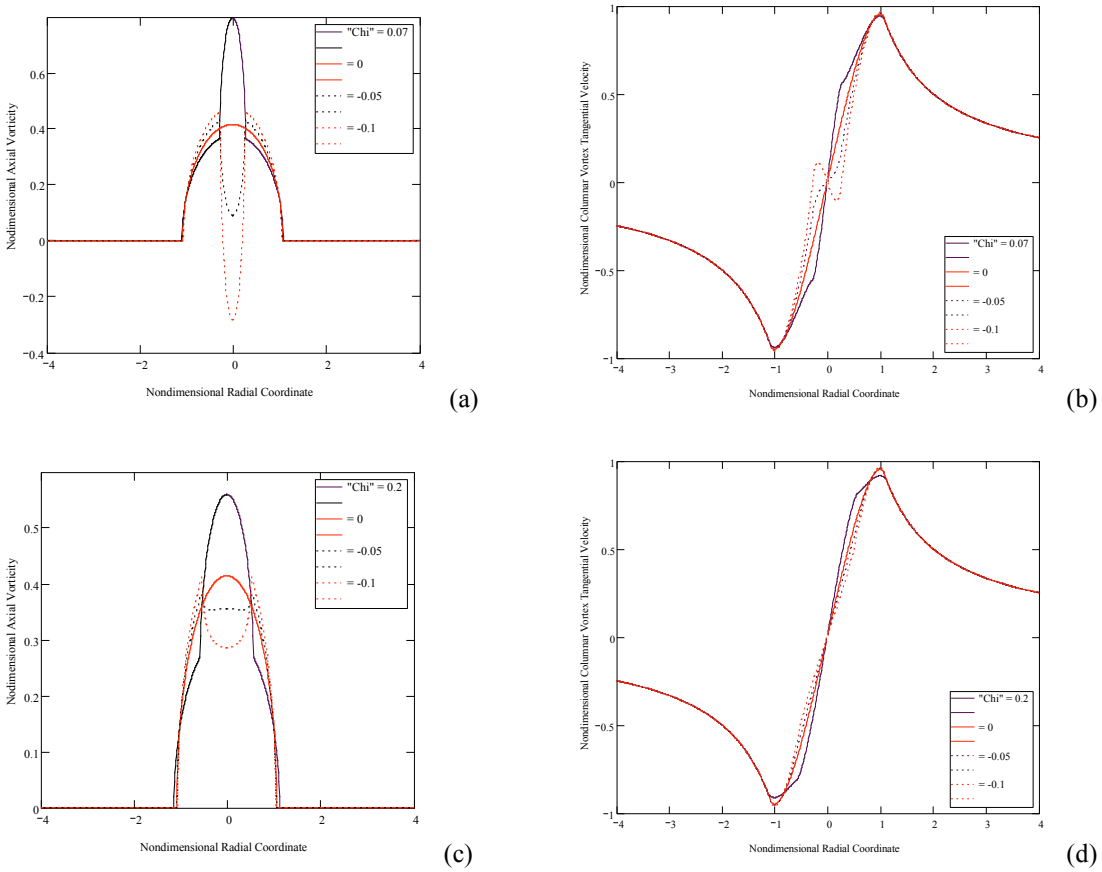

Fig. 1. Examples of Initial Vorticity and Velocity Distributions describable within Family of Vortices: (a) and (b) vorticity and velocity for various χ_A at $\eta_A = 0.25$; (c) and (d) vorticity and velocity for various χ_A at $\eta_A = 0.5$

A number of interesting, if not unusual, initial axial vorticity and tangential velocity distributions are incorporated in this family of vortices. (Unusual that is for the non-distorted vortices typically studied. For vortex filaments subjected to the strain and disruption of being "cut," or otherwise severely subjected to body-vortex interactions, such distorted velocity profiles may be the norm.) As a further aside, it should also be noted that the reason why the maximum nondimensional tangential velocity at $t = 0$ is not always equal to unity is because not all the vorticity is initially captured within the core of the vortex, as, in general, $r_{oA} > r_{c0A}$. Perhaps the most important attribute of this family of vortices is the ability to model inner regions of negative axial vorticity within the vortex core, the magnitude of which is finite at $t = 0$, and consequently modeling counter-rotating swirling flow near the vortex centerline. The ability to directly manipulate the appearance and initial extent of such inner regions of negative vorticity, with respect to the

vortex core, is essential in studying the influence of vortex breakdown phenomena during the course of vortex reconnection.

A. Time-Dependent Behavior of Columnar (Uncut) Vortices

The columnar vortex solutions are exact solutions to the laminar viscous Helmholtz vorticity equations. Figure 2a-d illustrates the time evolution of columnar vortices representing opposite extremes of the initial vorticity and velocity distributions studied in this paper. (Note that a factor of 2π has been applied to relate the nondimensional scaling employed in this paper to the conventional nondimensional scaling used for columnar vortices.) The tangential velocity profiles all slowly transition from their initial profiles to a Lamb-Oseen vortex profile with time. Also noteworthy, the counter-rotating swirl in the inner core stemming from negative vorticity can be clearly seen in Fig. 2c-d.

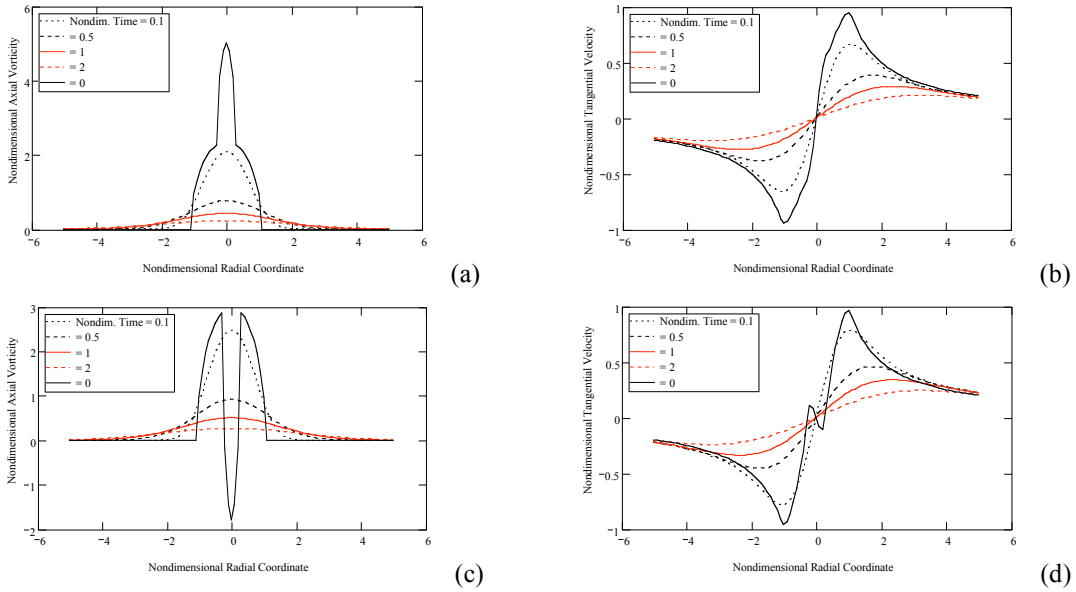

Fig. 2. Time Evolution of Two Different Columnar Vortices: (a-b) vorticity and velocity, $\chi_A = 0.07$ and $\eta_A = 0.25$, and (c-d) at $\chi_A = -0.1$ and $\eta_A = 0.25$

B. Reconnection and Breakdown for Semi-Infinite Filaments

As noted in Ref. 11 the general characteristics of axisymmetric vortex reconnection is predicted to include: (1) diffusion-like reestablishment of vortex circulation in the intermediate region(s) between breakpoints, (2) manifestation of "funnel-like" instantaneous stream function contours near the individual vortex filament breakpoints; (3) spiral patterns for particle traces and/or streaklines (spiraling in towards the vortex centerline and away from the breakpoint along the filament axis), (4) complex enstrophy contours early in the vortex reconnection process followed later by simple diffusion-like contours. Depending on the initial vorticity distribution (e.g. the "dual-core" model), the vortex reconnection process also sometimes exhibited – for a brief period of time – vortex breakdown bubbles. A more complete understanding of the conditions by which vortex breakdown phenomena are exhibited during the vortex reconnection process is of particular interest in this paper.

The existence or nonexistence of axisymmetric vortex breakdown bubbles can be established on the basis of whether or not stagnation points exist along the vortex centerline in the intermediate region between axial flow wave front boundaries. This can be established by the implicit relationship

$\delta \equiv \int_0^{z_w} v_z\big|_{r=0} dz - \int_0^{z_w} \left| v_z\big|_{r=0} \right| dz$, where ε is an error tolerance constant, such that $|\delta| > \varepsilon$ when the vortex breakdown bubble exists and $|\delta| \le \varepsilon$ when the bubble does not exist. This is merely an existence criterion, though. It does not provide any details as to the number and location of stagnation points in the vortex filament or any other characteristic of the bubble formation.

An alternate formulation, less computationally expensive, for approximately establishing the existence of vortex breakdown bubbles, which can also be used to define the duration, in terms of nondimensional time, t_{limit}, that the vortex bubbles exist, is given by the expression $v_z\Big|_{\substack{t=t_{limit} \\ |z|=(s+z_w)/2 \\ r\to 0}} \approx 0$. Estimates of this persistence of vortex bubbles during vortex reconnection is presented in Fig. 3 as a function of χ_A and η_A. The bubbles exist for a brief period of nondimensional time (typically $t^{\bullet} \le 0.06$) for those combinations of χ_A and η_A where negative axial vorticity exists in the inner core of the vortex.

Typically, though, a vortex breakdown criterion is defined in terms of swirl, or Rossby, number limits rather than the nondimensional time limits shown in Fig. 3. The Rossby number, Ro, is given by the relationship $Ro \equiv V/\Omega L$, where V and L are a characteristic velocity and length respectively, and Ω is a characteristic rotational rate of the flow. A vortex Rossby number can be cast in following terms $Ro = v_{z0}/r_{c0}\Omega$, where, in general $v_{z0} = v_z\big|_{r\to 0}$ and $\Omega = v_\theta / r\big|_{r\to 0}$. Further, specifically, the following approximate definitions are employed to define Fig. 4: first, $v_{z0} \approx v_z\big|_{r\to 0}\big|_{z=s/2}$ and, second, $\Omega \approx \left(v_\theta / r\right)\big|_{r\to \varphi r_{c0A}}\Big|_{z>>0}$ where $\varphi \approx 0.9$ (the constant φ is close to unity in value so as to estimate the rotational rate of the portion of the vortex external to inner counter-rotating swirling flow). Figure 4 shows a range of Rossby numbers, $Ro \approx 0.45 - 0.75$, whereby the vortex breakdown disappears during the vortex reconnection process. This is a unique treatment of the problem as most other research assesses the Rossby number limits in terms of when breakdown bubbles appear rather than disappear as is done in this study.

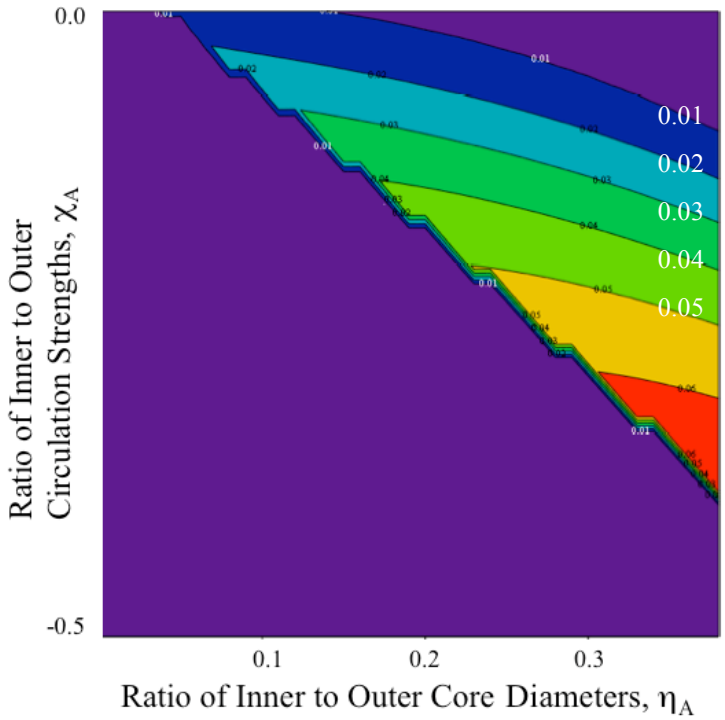

Fig. 3. Vortex Breakdown Manifestation: Nondimensional Time Boundaries

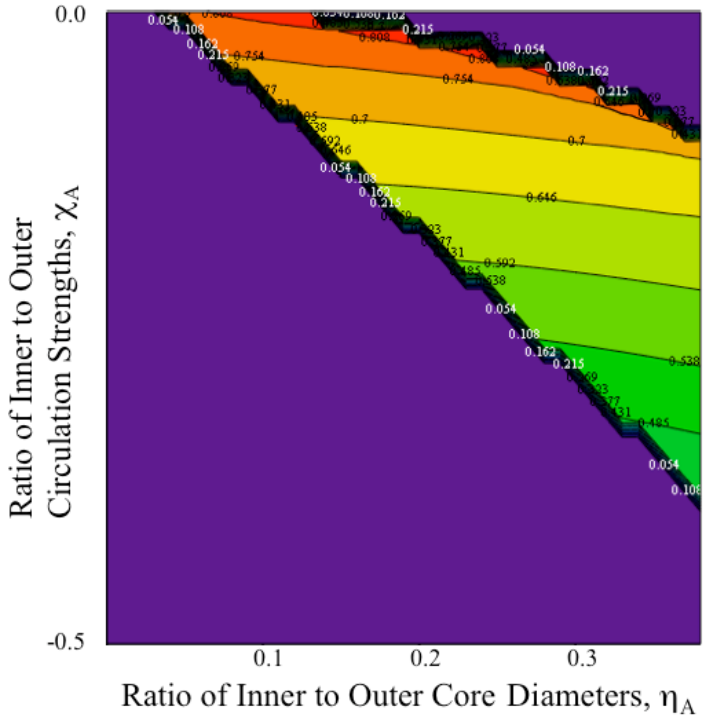

Fig. 4. Vortex Breakdown Manifestation: Rossby Number Limits

Figure 5 illustrates briefly the influence of initial vorticity distribution (refer to the Appendix for more details as to the analytical definition of the initial vorticity and velocity distributions for this family of vortices) on vortex core distribution, the rate that tangential velocity is reestablished across the intermediate regions between breakpoints, and the existence, or nonexistence, or vortex breakdown bubbles during the early stages of the vortex reconnection process. This is presented in Fig. 5 in terms of varying the inner core circulation strength parameter, χ_A, while keeping the values of η_A and t^* constant.

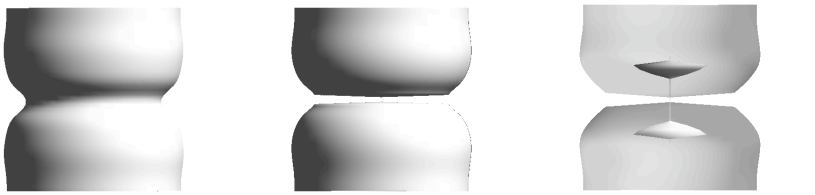

(a) (b) (c)

Fig. 5. Vortex Core (and Breakdown Bubble if Manifested) Distribution as a Function of Initial Vorticity Distribution ($\eta_A = 0.25$, $t^* = 0.01$, and Re=50): (a) , (b) , $\chi_A = 0$, i.e. "parabolic-core," (c) $\chi_A = -0.2$

One of the key results of this paper, over that presented in Refs. 10-11 for the "dual-core" vortex model, is that embedding negative vorticity in the vortex core does not manifest singularities in the vortex circulation distribution near the vortex breakpoints at very small value of time. Figure 6 clearly shows that there are no singularities exhibited at the vortex breakpoints for the new vortex model developed in this

paper that enables an improved characterization of "dual core" vortices or any vortices containing finite regions of negative vorticity in their inner core.

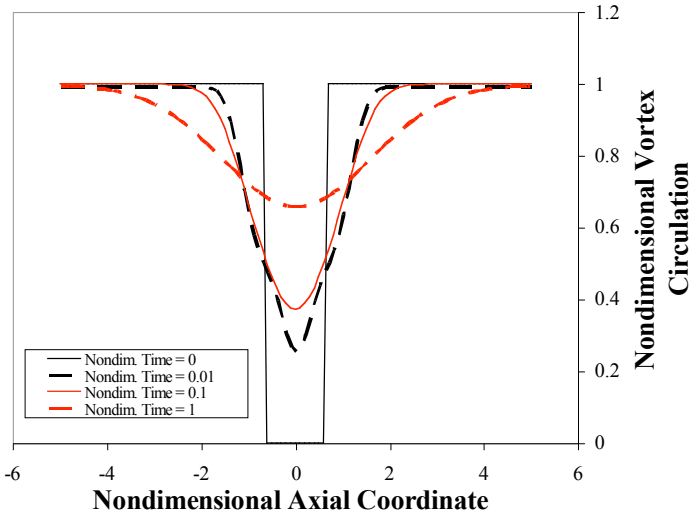

Fig. 6. Vortex Circulation Axial Distribution

The time dependent behavior of the predicted vortex breakdown is seen in Figs. 7-8. For $\chi_A = -0.3$ and $\eta_A = 0.375$, the vortical flow enstrophy and stream function contours are presented for a series of nondimensional times in Fig. 7. Figure 8 illustrates the temporal evolution of the vortex core and breakdown bubble envelopes for $\chi_A = -0.3$ and $\eta_A = 0.375$. It is particularly noteworthy to point out that the observed persistence of the bubble manifestation in Fig. 8 is consistent with the Fig. 3 curves.

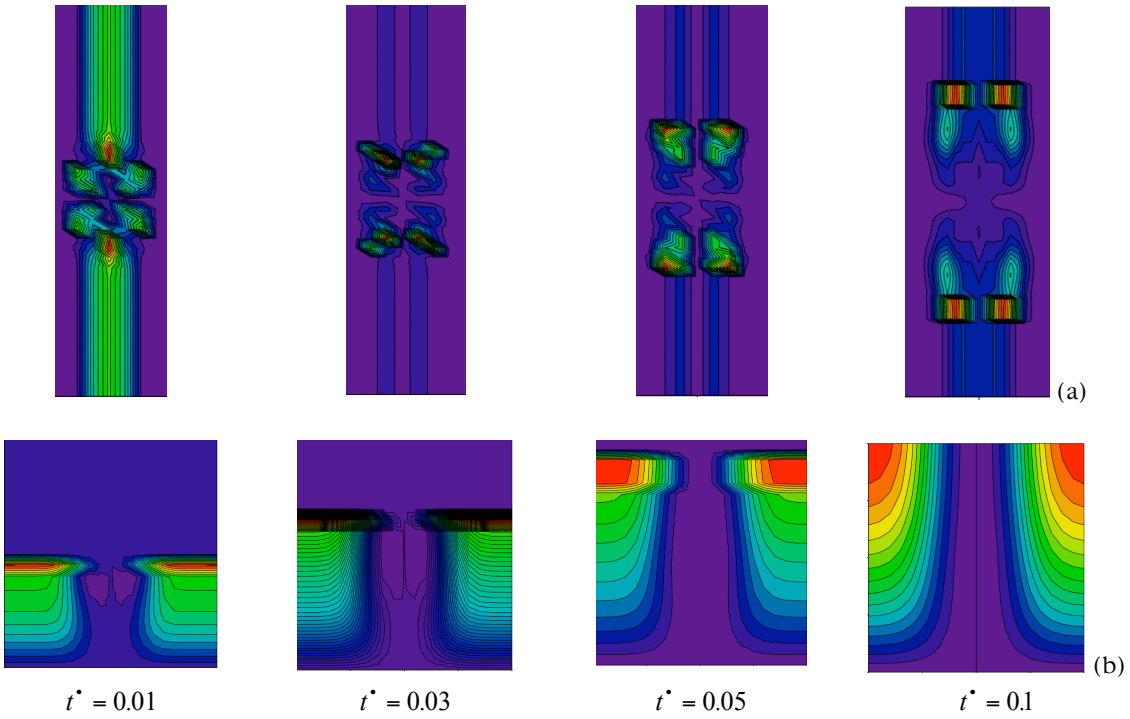

Fig. 7. Enstrophy and Instantaneous Stream Function Contours

Figure 8 illustrates in greater detail the time evolution of the predicted axisymmetric vortex breakdown bubbles manifested at the earliest stages of vortex reconnection (for those members of the family of vortices where negative axial vorticity is demonstrated). Two mirrored vortex breakdown bubbles are shown in the Fig. 8 predictions; this is because the flow is assumed symmetrical about the plane of symmetry midway between the vortex filament breakpoints. This is not an absolute requirement of the analysis presented in this paper; asymmetrical distributions can be accommodated in this analysis such that one, or two, or more vortex breakdown bubbles may be simulated in the vortical flow.

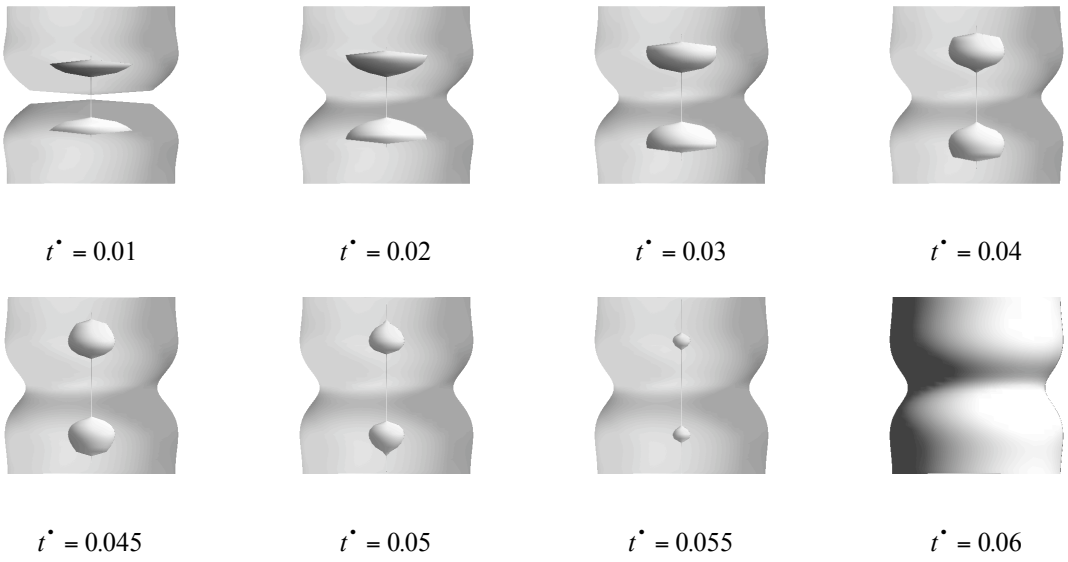

Fig. 8. Representative Vortex Breakdown Bubble Time Evolution

C. Influence of Finite Segments, i.e. "Seeds," of Negative Vorticity on Reconnection and Breakdown

Reference 10 and 11 performed initial analytical investigations into vortex filament reconnection and breakdown phenomena. In both references, inner cores of negative vorticity, as represented by a "dual core" initial vorticity distribution was sufficient to instigate vortex bubble formation and time evolution. However, this "dual core" vortex model had significant limitations to its utility. Many of these limitations have been rectified by the work presented in this paper. However, so far, the study of the influence of negative vorticity in the vortex core on axisymmetric vortex breakdown bubble formation has assumed that this negative vorticity is (semi-) infinite in span along the filament. This section of the paper will now study cases where either multiple cuts/breaks occur along the vortex filament or, alternatively, where negative vorticity is captured/embedded in finite span "seeds" inside vortex inner core. Such cases of finite regions of negative vorticity, near the vortex filament breakpoints, is likely to be more representative of physical realistic flow wherein the negative vorticity is generated, and entrained by the vortex filaments, as the vortex interacts with the boundary layer of a solid body/surface during the cutting process itself. Figure 9 illustrates the trends with respect to the resulting enstrophy contours of the axial "span" of the inner core negative vorticity region(s). In particular the creation of radial and azimuthal vorticity at the second wave front boundary, stemming from the "finiteness" of the axial span of the inner-core negative vorticity, can be clearly seen in Fig. 9.

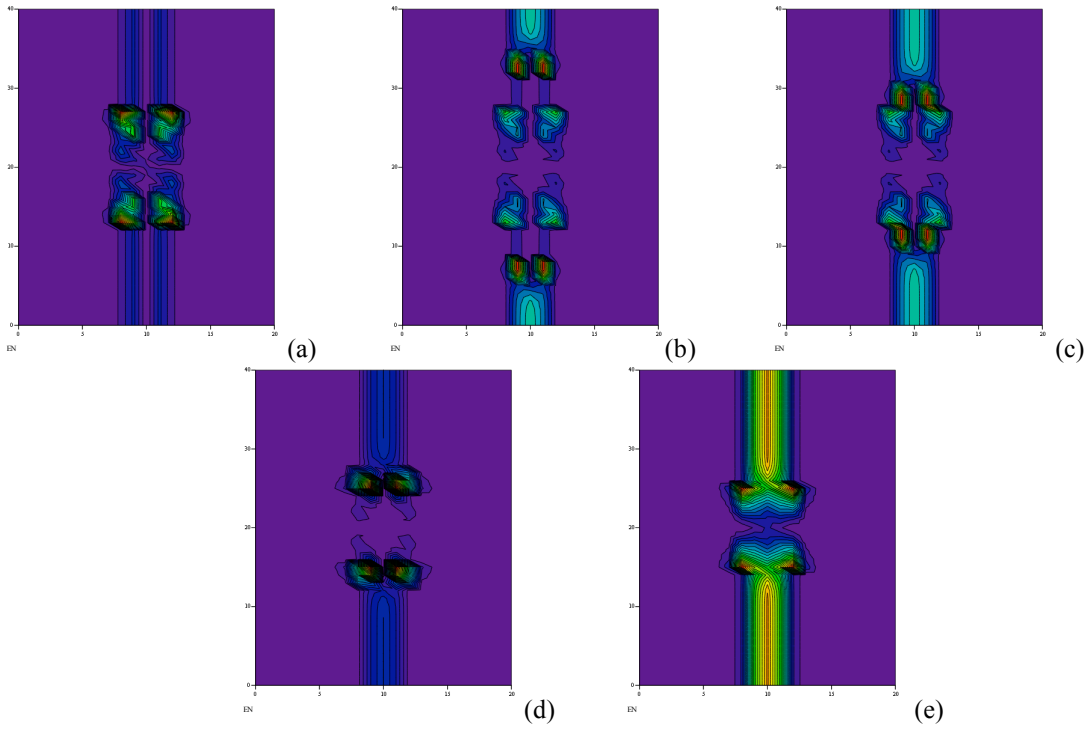

Fig. 9. Enstrophy Contours as a Function of Finite Span of Negative Vorticity "Seeds" in the Inner Core ($t^{\bullet} = 0.05$, $\chi_A = \chi_B = -0.3$, and $\eta_A = \eta_B = 0.375$): (a) $\ell_A / r_{c0A} = \ell_B / r_{c0B} = \infty^-$, (b) $\ell_A / r_{c0A} = \ell_B / r_{c0B} = 3$, (c) $\ell_A / r_{c0A} = \ell_B / r_{c0B} = 2$, (d) $\ell_A / r_{c0A} = \ell_B / r_{c0B} = 1$, and (e) $\ell_A / r_{c0A} = \ell_B / r_{c0B} = 0$ ("parabolic core")

It is reasonable to consider the question whether or not such "seeds" of negative vorticity, generated during a body-vortex-interaction, is sufficient to initiate formation of vortex breakdown phenomena. It is anticipated that the following general constraint applies – i.e. $|b_i - a_i| \geq V_P t_{lim}$ where t_{lim} can be numerically defined in the same manner as the time limits noted in Fig. 3 -- then vortex breakdown axisymmetric bubble formation and dissipation is essentially indistinguishable from that observed and noted earlier for semi-infinite expanses of negative vorticity in vortex cores. If the span of the region of negative vorticity is below this limit, i.e. $|b_i - a_i| < V_P t_{lim}$, such that $|b_i - a_i| << r_{c0A}$, then the persistence, even the existence, of vortex breakdown bubbles is significantly curtailed. This is clearly exemplified in Fig. 10 which reveals that the vortex breakdown bubble overall size, and geometry, is fairly constant for large spans of inner-core negative vorticity; however, as the finite span of the negative vorticity drops below a critical limit then the breakdown bubble begins to collapse prior to nominal nondimensional time limits shown in Fig. 3. Further, it is important to note that the "finiteness" of the axial span of the inner-core negative vorticity can also have an influence on the vortex core envelope, as well, as evidenced by comparing the vortex core envelope of Fig. 10a-b with the contour shown in Fig. 10c. The Fig. 10c core envelope varies to a greater degree for small or localized "seeds" of negative vorticity as compared to larger, or semi-infinite, distributions of negative vorticity.

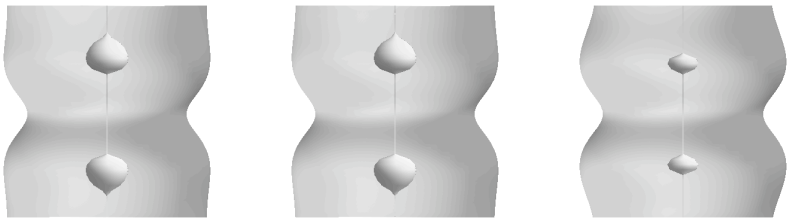

(a) (b) (c)

Fig. 10. Vortex Core and Breakdown Bubble Envelopes as a Function of Finite Span of Negative Vorticity "Seeds" in the Inner Core ($t^* = 0.05$, $\chi_A = \chi_B = -0.3$, and $\eta_A = \eta_B = 0.375$): (a) $\ell_A / r_{c0A} = \ell_B / r_{c0B} = 3$, (b) $\ell_A / r_{c0A} = \ell_B / r_{c0B} = 2$, and (c) $\ell_A / r_{c0A} = \ell_B / r_{c0B} = 1$

D. Approximate Influence of "Post-Cut" Variable Vortex Core Size

Experimental and computational observations, e.g. from Ref. 8, have revealed that the vortex filament core size is not constant, subsequent to being cut by a solid body, and varies along the span of the filament for columnar vortices having nonzero axial velocity in the vortex core prior to cutting. The upstream portion of the filament undergoes an expansion of the core (due to the axial flow being decelerated to zero during its cutting by the solid body) while the downstream portion of the core contract (both the expansion and contraction primarily occurs in the immediate vicinity of the cut).

Figure 11 is the vortex core evolution, with time, emulating the initial variable core size distributions observed, e.g. Ref. 8, for orthogonal blade cutting of vortices with nonzero axial flow. As this is only an approximate simulation/emulation of the experimentally observed vortex core distributions during orthogonal body-vortex interaction, only a qualitative appreciation of the time evolution of such vortices can be made. Nonetheless, even with this simple example, there is good general agreement with the overall flow features observed experimentally.

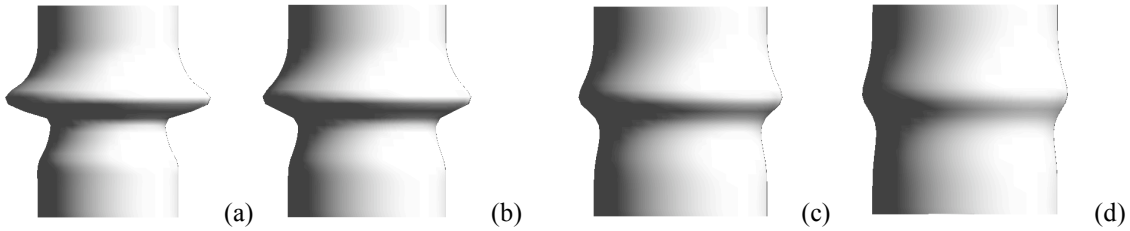

(a) (b) (c) (d)

Fig. 11. Time Evolution of an Initially Variable Core Size Axial Distribution: (a) $t^* = 0.05$, (b) $t^* = 0.1$, (c) $t^* = 0.2$, and (d) $t^* = 0.3$

Finally, it should be noted that this analytical work could also be applied to cases where not only "ideal cuts" (where there is no axial vorticity in the intermediate region between breakpoints) have been modeled but non-ideal filament "breaks" (where there is still non-negligible axial vorticity in the intermediate region) as well. Such analytical work, though not fundamentally changing the results presented, would represent a more physically realistic flow process.

E. Influence of Reynolds Number

The results in this paper are for the most part presented for low vortex Reynolds numbers, typically Re=50. In actuality, the columnar vortex and vortex reconnection solutions presented exhibit mostly independence with respect to Reynolds number, with the unique exception of the wave front boundary propagation velocity and, by extension, each boundary's spatial location. This, in turn, has a modest effect on the geometry of the vortex breakdown bubbles (and internal recirculation cell). Figure 12a-c presents instantaneous stream function contours, in the immediate vicinity of a vortex filament breakpoint, as a function of vortex Reynolds number (Re=100, 500, and 1000). Figure 12d illustrates the influence of employing large values of turbulent effective viscosity ($\nu_{eff} = \delta\nu$) in making the stream function predictions for higher Reynolds numbers; the net effect of the turbulent viscosity is to "age" the vortex with respect to the purely laminar vortex in the overall progression of the reconnection process. Figure 12e presented at an equivalent "effective" nondimensional time ($t^{\bullet}_{eff} \equiv \nu_{eff} t / r^2_{c0A}$) validates, though, that turbulent viscosity -- as to be expected given the previously note independence of the solution with respect to Reynolds number -- does not fundamentally alter either the character or orderly progression of the vortex reconnection process as compared to the laminar flow viscosity values. Employing turbulent viscosity will not, therefore, result in the manifestation of the large conical turbulent vortex breakdown "bubbles" observed in Ref. 12, for example. (The work of Ref. 12 would suggest that non-axisymmetric formulations of the Navier-Stokes or Helmholtz equations are required, to capture spiral modes/instabilities, to model the large turbulent conical vortex breakdown structures observed in that work. Such spiral modes, and associated phenomena, cannot be predicted with the axisymmetric solution presented in this paper.)

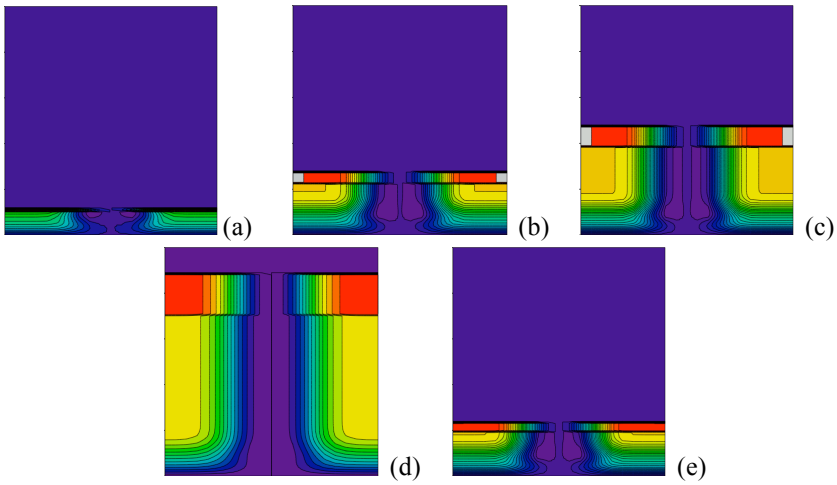

Fig. 12. Reynolds Number ($t^{\bullet} = 0.01$, $\chi_A = -0.3$, and $\eta_A = 0.375$): (a) Re=100, (b) Re=500, (c) Re=1000 ($|r| \le 2$ and $0 \le z \le 10$), (d) Re=2000 with effective turbulent viscosity ($\delta = 5$), and (e) Re=2000 ($t^{\bullet} = 0.002$ and $t^{\bullet}_{eff} = 0.01$)

The Reynolds number observations, noted above, have to be moderated when it comes to considering finite spans, versus semi-infinite distributions as shown in Fig. 13, of inner-core negative vorticity. As seen in Fig. 12, the vortex breakdown bubble axial expanse is somewhat "open-ended" with respect to Reynolds number for semi-infinite inner-core negative vorticity. In other words, for the semi-infinite negative vorticity distribution case, the bubble length increases without limit with increasing vortex Reynolds number. However, this does not hold for finite spans of inner-core negative vorticity. Under these circumstances, the bubble length is constrained, i.e. self-limiting, by the appearance of the second wave front boundary, to constrained to some maximum length that directly corresponds to the initial span of the inner-core negative vorticity region. This can be clearly seen in Fig. 13a-b where instantaneous stream function contours are presented for two different negative vorticity distributions. This result is a

particularly crucial one, as empirical observations of axisymmetric vortex breakdown bubbles tend to consist mostly low fineness ratio (length-to-diameter) bubbles.

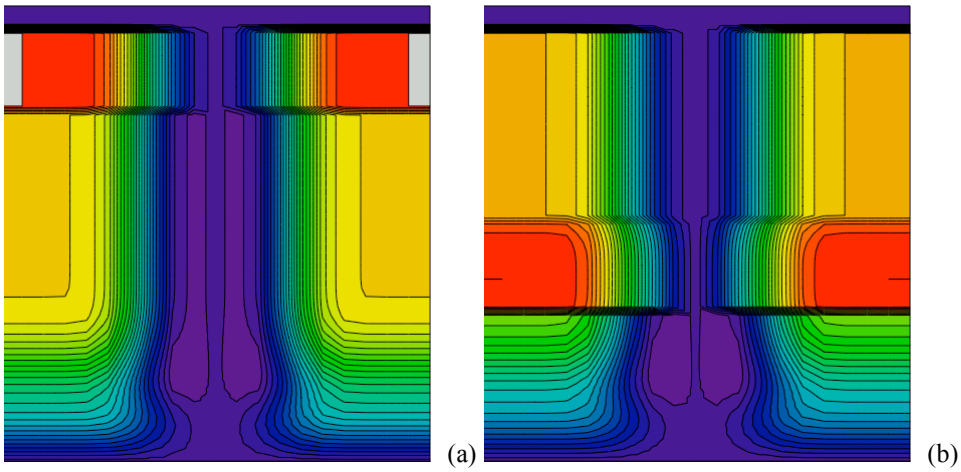

Fig. 13. Influence of Finite-Span, a.k.a "Seeds," of Negative Vorticity versus Semi-Infinite Distributions (Re=1000, $t^{*} = 0.01$, $\eta_A = 0.25$, and $\chi_A = -0.2$): (a) $\ell_A / r_{c0A} = \ell_B / r_{c0B} = \infty^{-}$ and (b) $\ell_A / r_{c0A} = \ell_B / r_{c0B} = 2$

F. Expanded Comments Related to Solution Approximations

There are four primary approximations inherent in the length scale factor methodology, in general, and the vortex reconnection solution, in particular. First, the idealization of the vortex reconnection problem as to being perfectly "cut," such that $\Gamma\big|_{r\to\infty} = 0$ at $t = 0$ for the intermediate regions between breakpoints, is in itself an approximation. In reality, such an "ideal cut," with corresponding total elimination of vorticity in the intermediate region prior to $t = 0$, is not possible. (Though no examples are provided in this paper, because of considerations with respect to brevity, the outlined analysis is capable of simulating non-ideal cuts, a.k.a vortex "breaks," wherein $\Gamma\big|_{r\to\infty} \neq 0$ within the intermediate region(s), though, $\Gamma\big|_{\substack{r\to\infty \\ z\approx 0}} << \Gamma\big|_{\substack{r\to\infty \\ |z|\to\infty}}$.) Second, an inherent outcome of the length scale factor for a fully three-dimensional problem is that, in addition to the fundamental assumptions of the methodology that $v_z = -\ell\omega_z$ and $v_r = -\ell\omega_r$, it is also ideally the case that $v_\theta \propto \omega_\theta$. In an approximate, but not exact sense, this proportionality is observed in the analytical solution. Third, the analytical expressions for all three vorticity components, and not just the axial vorticity, has to ideally satisfy the unsteady heat conduction equation cast in terms of each respective vorticity component, or, alternatively, an "infinite (large) Reynolds number" assumption has to be applied. Fourth, it should be noted there is no *a priori* characterization of the geometry of the wave front boundaries. A planar-wave type geometry for the wave front boundaries is assumed in this paper though alternate realizations might be more valid. Further, the propagation velocity of the wave boundaries is based on a simple approximate formula, rather than some exact treatment.

The impact of these approximations, to a first order, can be estimated. A "residual error" function will now be defined to help characterize the relative level of approximation in the vortex reconnection solution – i.e. $\boldsymbol{\varepsilon} \equiv D\boldsymbol{\omega}/Dt - (\boldsymbol{\omega}\cdot\nabla)\mathbf{V} - \nu\nabla^2\boldsymbol{\omega}$. If the solution were exact for all conditions and regions within the flow then $\boldsymbol{\varepsilon} = 0$. In fact, one component of the "residual error" function is indeed identically equal to zero as a consequence of the length scale factor methodology: i.e. $\varepsilon_z \equiv 0$. However, as illustrated in Fig. 14a-d,

the other two components, ε_θ and ε_r, are not identically zero for all conditions and vortical flow regions for the vortex reconnection solution, as typified by the "parabolic core," $\chi_A = 0$, model. For both cases, the nondimensionalized values for ε_θ and ε_r exhibit non-negligible nonzero values near the vortex centerline in the intermediate region for small values of nondimensional time and low vortex Reynolds numbers. In particular, ε_θ, derived from the azimuthal vorticity equation, exhibits by far the largest residual error values (by at least an order of magnitude near the vortex centerline in the intermediate region between breakpoints). This is almost exclusively the case because the $\left(\partial\omega_\theta/\partial r\right)/r$ term in the Laplacian operator is not identically canceled out by the contribution of the other terms at the vortex axis, thus exhibiting a singularity at $r = 0$ with the "parabolic core" vortex reconnection solution -- and, by extension, the rest of the family of vortices presented in this paper.

As Reynolds number increases the residual error correspondingly decreases (e.g. Fig. 14c-d) though areas of residual error other than the localized region near the vortex centerline now become more obvious. The vortex reconnection solution may, perhaps, be considered a "large Reynolds number" solution (though clearly not inviscid) even though imposing a "large Reynolds number" assumption was not explicit in the solution derivation. This perhaps best evidenced by the (for the most part) Reynolds number independence exhibited in the vortex reconnection solutions (with the key exception being the wave front boundary location and propagation velocity); otherwise, Reynolds number merely affects the spatiotemporal scaling of the problem and not the exhibited phenomenology itself. Additionally, as nondimensional time increases the observed residual error decreases as seen in Fig. 14e-f.

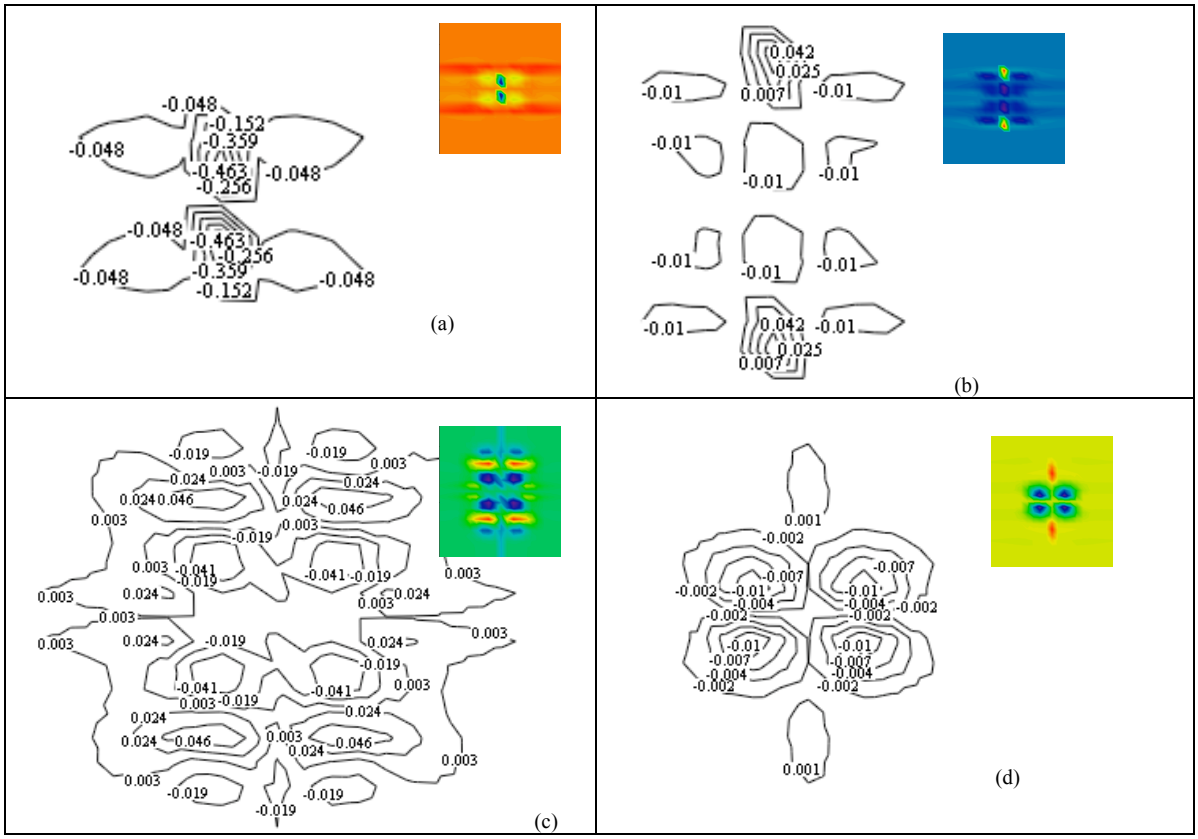

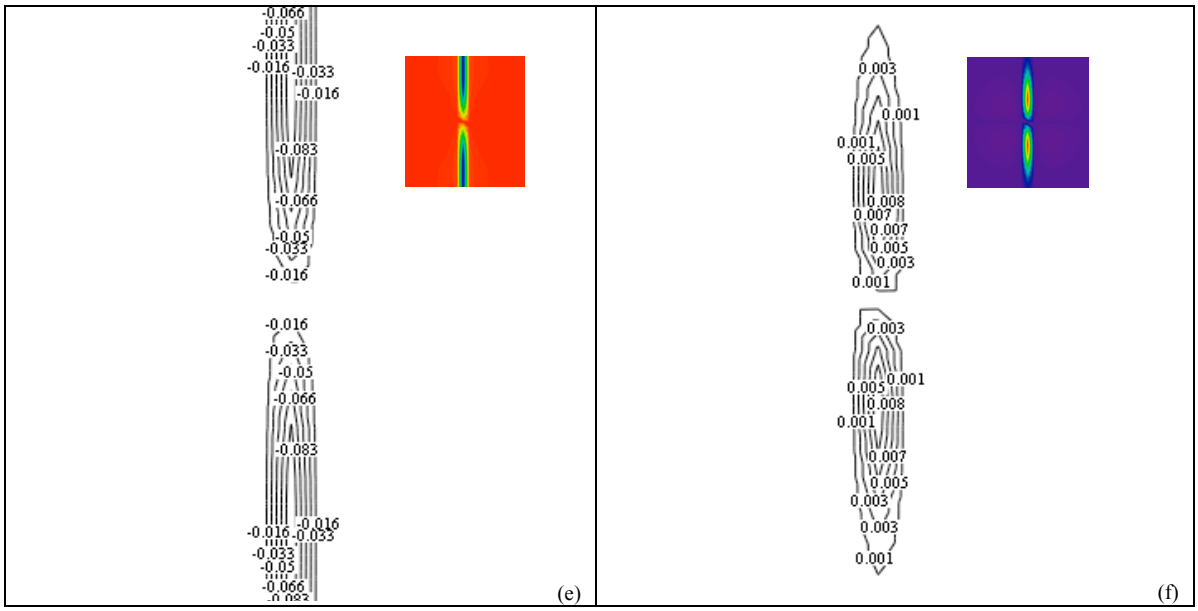

Fig. 14. Approximation with respect to Viscous Helmholtz Equation: (a) Residual Error for Azimuthal Vorticity, ε_θ, and (b) Residual Error for Radial Vorticity, ε_r ($t^\bullet = 0.1$ and Re=50); (c) ε_θ and (d) ε_r ($t^\bullet = 0.1$ and Re=1000); (e) ε_θ and (f) ε_r ($t^\bullet = 1$ and Re=50)

It is important to note that in the above discussion that "residual error" is not synonymous with absolute error. The residual error results merely reflect where, when, and how the derived analytical solutions do not exactly satisfy the Helmholtz equations. The residual error estimates do not, however, quantify the accuracy of the approximation. For example, it is quite conceivable that a relatively small inaccuracy in predicting ω_θ or ω_r at the vortex centerline can potentially result in a large residual error estimate if the $(\partial\omega_\theta/\partial r)/r$ and $(\partial\omega_r/\partial r)/r$ contributions are not exactly canceled out by the collective contributions from the vorticity time derivatives and the other Laplacian operator terms. Having performed this initial assessment of the level of approximation inherent in the derived solution, it bears repeating that the analysis outlined in this paper, though of approximate nature, is nonetheless of great utility in understanding vortical flow phenomena as diverse as vortex breakdown and vortex reconnection.

Concluding Remarks

A new family of laminar vortices has been analytically derived. These vortices can be studied as either columnar vortices or vortex filaments undergoing vortex reconnection and breakdown. The columnar vortex solutions represent exact solutions for the Helmholtz vorticity equations. The vortex reconnection solutions, in turn, are only approximate in nature, but provide fully three-dimensional, though axisymmetric, analytic insight into very complex flow phenomenon. In particular, the presence of negative axial vorticity (both in terms of strength and distribution) in the inner core of vortex filaments has a profound effect on the manifestation and persistence of axisymmetric vortex breakdown bubbles in the early stages of vortex reconnection, as well as influencing the bubble geometry. Correspondingly the influence of vortex Reynolds number, including the application of turbulent effective viscosity to simulate mean turbulent flow, is investigated as to the vortex reconnection phenomenon. As predicted by the analysis, the Reynolds number primarily influences the spatiotemporal scaling of the flow but has little effect on the general types of flow behavior manifested. In this regards, the vortex solutions exhibit a large degree of Reynolds number independence, thereby lending additional support to the supposition that the

derived laminar analysis results can also potentially provide insight into turbulent vortical flow through selective application of turbulent effective viscosity.

The presented analytical work can be readily extended to consider active flow control approaches whereby the primary vortical flow is disrupted in a periodic or pulsed manner by either vortex "cutting" or injection/entrainment of negative vorticity into the vortex inner core. Such active flow control approaches to vortex modification for rotary- and fixed-wing applications has been long sought after, but not yet robustly demonstrated, primarily because of the need for an improved understanding of the fundamental physics of vortical flow phenomenon.

References

[1]Spencer, R.H., "Application of Vortex Visualization Test Techniques to Rotor Noise Research," 26th Annual Forum of the American Helicopter Society, Philadelphia, PA, June 1970.

[2]Fontana, R.R. and Hubbard, Jr., J.E., "A Comparison with Theory of Peak to Peak Sound Level for a Model Helicopter Rotor Generating Blade Slap at Low Tip Speeds," Ninth European Rotorcraft and Powered Lift Aircraft Forum, Stresa, Italy, September 1983.

[3]Swanson, A.A., "Application of the Shadowgraph Flow Visualization Technique to a Full-Scale Helicopter Rotor in Hover and Forward Flight," AIAA-93-3411, AIAA 11'th Applied Aerodynamics Conference, Monterey, CA, August, 1993.

[4]Light, J.S., Swanson, A.A., and Norman, T.R., "Application of the Wide-Field Shadowgraph Technique to Helicopters in Forward Flight," Journal of the American Helicopter Society, Vol. 37-No. 2, April 1992.

[5]Crouse Jr., G.L., Leishman, J.G., and Bi, N., "Theoretical and Experimental Study of Unsteady Rotor/Body Aerodynamic Interactions," Journal of the American Helicopter Society, Vol. 37-No. 1, January 1992.

[6]Foley, S.M., Funk, R.B., Fawcett, P.A., and Komerath, N.M., "Rotor-Wake-Induced Flow Separation on a Lifting Surface," Journal of the American Helicopter Society, Vol. 40-No. 2, April 1995.

[7]Brand, A., Komerath, N., and McMahon, H., "Results from Laser Sheet Visualization of a Periodic Rotor Wake," AIAA Journal of Aircraft, Vol. 26-No. 5, May 1989.

[8]Marshall, J.S., "Vortex Cutting by a Blade, Part 1: General Theory and a Simple Solution," AIAA Journal, Vol. 32, No. 6, June 1994.

[9]Weigand, A., "The Response of a Vortex Ring to a Transient Spatial Cut," Proceedings of the Seventh International Symposium on Flow Visualization, Ed. J. Crowder, Seattle, WA, September 1995.

[10]Young, L.A., "Vortex Flow Behavior Subsequent to Perpendicular Collision with a Solid Body," Soon to be published NASA TM.

[11]Young, L.A., "Influence of Initial Vorticity Distribution on Axisymmetric Vortex Breakdown and Reconnection," AIAA-2007-1283, 45th AIAA Aerospace Sciences Meeting, Reno, NV, January 8-11, 2006.

[12]Novak, F. and Sarpkaya, T. "Turbulent Vortex Breakdown at High Reynolds Numbers," AIAA 99-0135, 37th AIAA Aerospace Sciences Meeting, Reno, NV, January 11-14, 1999.

[13]Carslaw, H.S. and Jaeger, J.C., Conduction of Heat in Solids, Second Edition, Clarendon Press, Oxford, 1959.

[14]Abramowitz, M. and Stegun, I.A., *Handbook of Mathematical Functions with Formulas, Graphs, and Mathematical Tables*, AMS 55, U.S. Department of Commerce, November 1967.

[15]Prudnikov, A.P., Brychkov, Y.A., and Marichev, O.I., (Queen, N.M., Trans.), Integrals and Series, Volume 1: Elementary Functions, Gordon and Breach Science Publishers, New York, 1988.

[16]Lamb, H., Hydrodynamics, Sixth Edition, Dover Publications, New York.

Appendix – Finite-Core Line Sources

Reference 13 summarized the exact solution for a finite (spherical) volume source, Eq. 15. Note that the parameter, r_o, is the spherical source terms radius. This parameter is related to the finite-core vortex filament initial core radius, r_{c0}, through consideration of the initial velocity and vorticity distributions, as detailed later.

$$\omega_z\Big|_{\substack{Finite\ Volume\\ Source}} = \frac{3\gamma}{8\pi r_o^3}\left\{ erf\left(\frac{\sqrt{r^2+(z-z_*)^2}+r_o}{2\sqrt{\nu t}}\right) - erf\left(\frac{\sqrt{r^2+(z-z_*)^2}-r_o}{2\sqrt{\nu t}}\right) - \frac{2\sqrt{\nu t}}{\sqrt{\pi\left(r^2+(z-z_*)^2\right)}}\left[e^{-\left(\sqrt{r^2+(z-z_*)^2}-r_o\right)^2/4\nu t} - e^{-\left(\sqrt{r^2+(z-z_*)^2}+r_o\right)^2/4\nu t}\right]\right\} \tag{15}$$

This finite volume source model is now applied to the following integral equation to define the incremental vorticity contribution, $\Delta\omega_z(\gamma, r_o, a, b)$, for a finite (or semi-infinite) span of finite-core line source.

$$\Delta\omega_z(\gamma, r_o, a, b, r, z, t) = \int_a^b \left(\omega_z\Big|_{\substack{Finite\ Volume\\ Source}}\right) dz_* \tag{16}$$

This becomes

$$\begin{aligned}&\Delta\omega_z(\gamma, r_o, a, b, r, z, t) = \\ &\frac{3\gamma}{8\pi r_o^3}\int_a^b erf\left(\frac{\sqrt{r^2+(z-z_*)^2}+r_o}{2\sqrt{\nu t}}\right)dz_* - \frac{3\gamma}{8\pi r_o^3}\int_a^b erf\left(\frac{\sqrt{r^2+(z-z_*)^2}-r_o}{2\sqrt{\nu t}}\right)dz_* \\ &-\frac{3\gamma}{4r_o^3}\sqrt{\frac{\nu t}{\pi^3}}\int_a^b \frac{e^{-\left(\sqrt{r^2+(z-z_*)^2}-r_o\right)^2/4\nu t}}{\sqrt{r^2+(z-z_*)^2}}dz_* + \frac{3\gamma}{4r_o^3}\sqrt{\frac{\nu t}{\pi^3}}\int_a^b \frac{e^{-\left(\sqrt{r^2+(z-z_*)^2}+r_o\right)^2/4\nu t}}{\sqrt{r^2+(z-z_*)^2}}dz_*\end{aligned} \tag{17}$$

The integral terms in Eq. 17 do not appear initially to be analytically tractable (except for the special case of defining the initial, $t = 0$, vorticity distribution). Stepping back a bit with respect to the radial integration of the finite-volume core source, and reconsidering the arrangement of terms

$$\begin{aligned}&\Delta\omega_z(\gamma, r_o, a, b, r, z, t) = \\ &\frac{3\gamma}{8r_o^3\sqrt{\pi^3\nu t}}\int_a^b \frac{1}{\sqrt{r^2+(z-z_*)^2}}\int_0^{r_o} r_*\left[e^{-\left(\sqrt{r^2+(z-z_*)^2}-r_*\right)^2/4\nu t} - e^{-\left(\sqrt{r^2+(z-z_*)^2}+r_*\right)^2/4\nu t}\right]dr_*dz_*\end{aligned} \tag{18}$$

Expanding the exponential terms and rearranging gives

$$\Delta\omega_z\left(\gamma,r_o,a,b,r,z,t\right)=$$
$$\frac{3\gamma}{8r_o^3\sqrt{\pi^3\nu t}}\left\{\int_a^b \frac{e^{-\left(r^2+\left(z-z_*\right)^2\right)/4\nu t}}{\sqrt{r^2+\left(z-z_*\right)^2}}\int_0^{r_o} r_* e^{-r_*^2/4\nu t}\left[e^{\left(2r_*\sqrt{r^2+\left(z-z_*\right)^2}\right)/4\nu t}-e^{-\left(2r_*\sqrt{r^2+\left(z-z_*\right)^2}\right)/4\nu t}\right]dr_*dz_*\right\}$$

(19)

Noting that the definition of the hyperbolic sine function is $\sinh u=\left(e^u-e^{-u}\right)/2$; therefore, the above can be recast as

$$\Delta\omega_z\left(\gamma,r_o,a,b,r,z,t\right)=$$
$$\frac{3\gamma}{4r_o^3\sqrt{\pi^3\nu t}}\left\{\int_a^b \frac{e^{-\left(r^2+\left(z-z_*\right)^2\right)/4\nu t}}{\sqrt{r^2+\left(z-z_*\right)^2}}\int_0^{r_o} r_* e^{-r_*^2/4\nu t}\sinh\left(r_*\sqrt{r^2+\left(z-z_*\right)^2}/2\nu t\right)dr_*dz_*\right\}$$

(20)

Note that $\sinh\left(cx\right)=\sqrt{\pi cx/2}\cdot I_{+1/2}\left(cx\right)$ (see, e.g. Ref. 14). The emergence of Bessel functions in the above equation based on cylindrical/polar coordinates is not unexpected. It is well known that Bessel functions are particular solutions of the unsteady heat conduction equation in cylindrical coordinates.

A series approach will now be taken to derive the solution of the above equation. Uniform convergence will be assumed for the series such that term-by-term integration can be performed. Given the series definition of the hyperbolic sine function

$$\sinh x=x+\frac{x^3}{3!}+\frac{x^5}{5!}+\frac{x^7}{7!}+\cdots+\frac{x^{2n+1}}{\left(2n+1\right)!}+\cdots \qquad \text{For } |x|<\infty \qquad (21)$$

Note the above limit of application of the series representation of the hyperbolic sine function. When $t=0$ then identically $x=\infty$ thus approaching the limit of application of this series representation of the hyperbolic sine function, i.e. $|x|<\infty$; this is the principal reason why the resulting flow solution is semi-convergent as $t\to 0$. Dealing with this issue of how to define the initial vorticity and velocity distributions is discussed later in the Appendix; not unexpectedly, it requires solving the axial vorticity expression, at $t=0$, prior to the hyperbolic sine series representation substitution.

Substituting the above series expression into the above integral equation eliminates the square-root terms

$$\Delta\omega_z\left(\gamma,r_o,a,b,r,z,t\right)=$$
$$\frac{3\gamma}{8r_o^3\sqrt{\left(\pi\nu t\right)^3}}\left\{\int_a^b e^{-\left(r^2+\left(z-z_*\right)^2\right)/4\nu t}\int_0^{r_o} r_* e^{-r_*^2/4\nu t}\left(\sum_{n=0}^{\infty} r_*^{2n+1}\frac{\left(\left(r^2+\left(z-z_*\right)^2\right)/\left(2\nu t\right)^2\right)^n}{\left(2n+1\right)!}\right)dr_*dz_*\right\}$$

(22)

Recasting the above in the form of a new function (basically a modification of the series function(s) defined in Ref. 10) gives

$$\Delta\omega_z(\gamma,r_o,a,b,r,z,t)=\frac{3\gamma}{8r_o^3\sqrt{(\pi\nu t)^3}}D_0(r_o,a,b,r,z,t)$$

(23)

Where

$$D_0(r_o,a,b,r,z,t)\equiv$$
$$\int_a^b\int_0^{r_o}\left(\sum_{n=0}^{\infty}r_*^{2(n+1)}e^{-r_*^2/4\nu t}\cdot\frac{\left(\left(r^2+(z-z_*)^2\right)/(2\nu t)^2\right)^n}{(2n+1)!}e^{-\left(r^2+(z-z_*)^2\right)/4\nu t}\right)dr_*dz_*$$

(24)

Noting the following integration formula from Ref. 15

$$\int x^{2m}e^{-a^2x^2}dx=-(2m-1)!!\frac{x^{2m-1}e^{-a^2x^2}}{2a^2}\sum_{k=0}^{m-1}\frac{1}{2^k(2m-2k-1)!!(ax)^{2k}}+\frac{\sqrt{\pi}(2m-1)!!}{2^{m+1}a^{2m+1}}erf(ax)$$

(25)

Note, from Ref. 15, the notation

$$n!!=\begin{cases}(2k)!!\\(2k+1)!!\end{cases}\qquad\text{Where}\qquad\begin{aligned}(2k)!!&=2\cdot4\cdot6\ldots(2n)=2^k k!\\(2k+1)!!&=1\cdot3\cdot5\ldots(2k+1)=\frac{2^{k+1}}{\sqrt{\pi}}\Gamma\left(n+\frac{3}{2}\right)\end{aligned}$$

With $0!!=(-1)!!=1$.

(26)

This integral formula applied to the $D_0(r_o,a,b,r,z,t)$ expression yields

$$D_0(r_o,a,b,r,z,t)=\nu t\cdot\int_a^b\left(\sum_{n=0}^{\infty}\left(D_{00}(n,r_o,t)-D_{00}\left(n,0^+,t\right)\right)\cdot\left(\frac{r^2+(z-z_*)^2}{(2\nu t)^2}\right)^n e^{-\left(r^2+(z-z_*)^2\right)/4\nu t}\right)dz_*$$

(27)

Where

$$D_{00}(n,\alpha,t)\equiv\frac{(2n+1)!!}{(2n+1)!}\left\{2^{n+1}\sqrt{\pi}(\nu t)^{n+1/2}erf\left(\alpha/2\sqrt{\nu t}\right)-2\alpha^{2n+1}e^{-\alpha^2/4\nu t}\sum_{k=0}^{n}\frac{2^k\left(\sqrt{\nu t}/\alpha\right)^{2k}}{(2n-2k+1)!!}\right\}$$

(28)

Recasting Eq. 27 slightly, and making the substitution $x = z - z_*$ and $dz_* = -dx$ with the associated change in integration limits, gives

$$D_0(r_o,a,b,r,z,t) = \nu t e^{-r^2/4\nu t} \cdot \int_{z-b}^{z-a} \left(\sum_{n=0}^{\infty} \frac{\left(D_{00}(n,r_o,t) - D_{00}\left(n,0^+,t\right)\right)}{(2\nu t)^{2n}} \cdot \left(r^2 + x^2\right)^n e^{-x^2/4\nu t} \right) dx \tag{29}$$

Series expansion of the n[th] power polynomial term needs to be performed. This is accomplished by use of the Binomial Theorem (see e.g. Ref. 14).

$$(a+b)^n = a^n + \binom{n}{1} a^{n-1}b + \binom{n}{2} a^{n-2}b^2 + \binom{n}{3} a^{n-3}b^3 + \ldots + b^n \tag{30a}$$

Where the binomial coefficients are defined by the relationship

$$\binom{n}{k} = \frac{n!}{(n-k)!\,k!} \tag{30b}$$

The Binomial Theorem expansion applied to the vorticity function yields

$$D_0(r_o,a,b,r,z,t) = \nu t e^{-r^2/4\nu t} \cdot \int_{z-b}^{z-a} \left(\sum_{n=0}^{\infty} \frac{\left(D_{00}(n,r_o,t) - D_{00}\left(n,0^+,t\right)\right)}{(2\nu t)^{2n}} \cdot \sum_{j=0}^{n} \frac{n!}{(n-j)!\,j!} r^{2(n-j)} x^{2j} e^{-x^2/4\nu t} \right) dx \tag{31}$$

Proceeding with the integration of the above with respect to x gives

$$D_0(r_o,a,b,r,z,t) = \nu t e^{-r^2/4\nu t} \cdot \sum_{n=0}^{\infty} \frac{1}{(2\nu t)^{2n}} \left(D_{00}(n,r_o,t) - D_{00}\left(n,0^+,t\right)\right)\left(D_{01}(n,b,r,z,t) - D_{01}(n,a,r,z,t)\right) \tag{32}$$

Where the second function, $D_{01}(n,\alpha,r,z,t)$, is defined as

$$D_{01}(n,\alpha,r,z,t) \equiv -\sum_{j=0}^{n} \frac{n!(2j-1)!!}{(n-j)!\,j!} r^{2(n-j)} \cdot \left\{ \sqrt{\pi} \cdot 2^j (\nu t)^{j+1/2} erf\left(\frac{z-\alpha}{2\sqrt{\nu t}} \right) - 2\nu t (z-\alpha)^{2j-1} e^{-(z-\alpha)^2/4\nu t} \cdot \sum_{m=0}^{j-1} \frac{\left(2\sqrt{\nu t}/(z-\alpha)\right)^{2m}}{2^m (2j-2m-1)!!} \right\} \tag{33}$$

Note that, in the above, the convention is assumed wherein $\sum_{m=0}^{k} x_m = 0$ when $k < 0$ and $\sum_{m=0}^{k} x_m = x_0$ when $m = k = 0$.

Next, defining a new function, $D_1(n,\alpha,\beta,z,t)$, where

$$D_1(n,\alpha,\beta,z,t) \equiv \lim_{r\to\beta} \int D_{01}(n,\alpha,\beta,z,t) r e^{-r^2/4\nu t} dr \tag{34}$$

Substituting for $D_{01}(n,\alpha,\beta,z,t)$, Eq. 33, in the expression for $D_1(n,\alpha,\beta,z,t)$, Eq. 34, gives

$$D_1(n,\alpha,\beta,z,t) \equiv \lim_{r\to\beta} \int \sum_{j=0}^{n} \frac{n!(2j-1)!!}{(n-j)!\,j!} D_{10}(j,\alpha,z,t) r^{2(n-j)+1} e^{-r^2/4\nu t} dr$$

With

$$D_{10}(j,\alpha,z,t) \equiv \left\{ 2\nu t (z-\alpha)^{2j-1} e^{-(z-\alpha)^2/4\nu t} \cdot \sum_{m=0}^{j-1} \frac{\left(2\sqrt{\nu t}/(z-\alpha)\right)^{2m}}{2^m (2j-2m-1)!!} - \sqrt{\pi} \cdot 2^j (\nu t)^{j+1/2} erf\left(\frac{z-\alpha}{2\sqrt{\nu t}}\right) \right\} \tag{35a-b}$$

Noting the following integral formula from Ref. 15

$$\int x^{2m+1} e^{-a^2x^2} dx = -\frac{x^{2m} e^{-a^2x^2}}{2a^2} \cdot \sum_{k=0}^{m} \frac{m!}{(m-k)!(ax)^{2k}} \tag{36}$$

Using the above integration formula, the function $D_1(n,\alpha,\beta,z,t)$, Eq. 35a, becomes

$$D_1(n,\alpha,\beta,z,t) \equiv -2\nu t \cdot \sum_{j=0}^{n} \frac{n!(2j-1)!!}{(n-j)!\,j!} D_{10}(j,\alpha,z,t) \beta^{2(n-j)} e^{-\beta^2/4\nu t} \cdot \sum_{k=0}^{n-j} \frac{(n-j)!\left(2\sqrt{\nu t}/\beta\right)^{2k}}{(n-j-k)!} \tag{37}$$

The tangential velocity distribution can be derived from the axisymmetric flow vorticity divergence relationship

$$\omega_z = \frac{\partial v_\theta}{\partial r} + \frac{v_\theta}{r} \tag{38}$$

Which implies the first-order ordinary differential equation

$$\frac{d}{dr}(\Delta v_\theta) + P(r)\Delta v_\theta = Q(r) \tag{39}$$

Where, for this particular case,

$$P(r) = 1/r$$

$$Q(r) = \Delta\omega_z = \frac{3\gamma}{8r_o^3\sqrt{(\pi\nu t)^3}} D_0(r_o,a,b,r,z,t)$$

(40a-b)

The general solution of this differential equation is

$$\Delta v_\theta(\gamma,r_o,a,b,r,z,t) = \frac{3\gamma}{8r_o^3\sqrt{(\pi\nu t)^3}\cdot r}\left\{\int D_0(r_o,a,b,r,z,t)rdr + C\right\}$$

(41)

Employing the function, $D_1(n,\alpha,\beta,z,t)$, Eq. 37, the incremental tangential velocity can be expressed

$$\Delta v_\theta(\gamma,r_o,a,b,r,z,t) = \frac{3\gamma}{8r_o^3\sqrt{\pi^3\nu t}\cdot r}\left\{\sum_{n=0}^{\infty}\frac{1}{(2\nu t)^{2n}}\left(D_{00}(n,r_o,t) - D_{00}\left(n,0^+,t\right)\right)\left(D_1(n,b,r,z,t) - D_1(n,a,r,z,t)\right) + C\right\}$$

(42)

Now noting that the integration constant, C, is derived by the boundary constraint that $v_\theta = 0$ at $r = 0$, which in turn implies that $\Delta v_\theta = 0$ at $r = 0$, therefore, the incremental tangential velocity expression is given by

$$\Delta v_\theta(\gamma,r_o,a,b,r,z,t) = \frac{3\gamma}{8r_o^3\sqrt{\pi^3\nu t}\cdot r}\cdot\left\{\sum_{n=0}^{\infty}\frac{1}{(2\nu t)^{2n}}\left(D_{00}(n,r_o,t) - D_{00}\left(n,0^+,t\right)\right)\cdot\left[\left(D_1(n,b,r,z,t) - D_1\left(n,b,0^+,z,t\right)\right) - \left(D_1(n,a,r,z,t) - D_1\left(n,a,0^+,z,t\right)\right)\right]\right\}$$

(43)

The radial vorticity component can be found from the following relationship (noting θ-symmetry)

$$\omega_r = \frac{1}{r}\frac{\partial v_z}{\partial\theta} - \frac{\partial v_\theta}{\partial z} = -\frac{\partial v_\theta}{\partial z}$$

(44)

Which, in turn, implies that the incremental radial vorticity can be derived from

$$\Delta\omega_r = -\frac{\partial}{\partial z}(\Delta v_\theta)$$

(45)

Which gives

$$\Delta\omega_r(\gamma,r_o,a,b,r,z,t) = \frac{-3\gamma}{8r_o^3\sqrt{\pi^3\nu t}\cdot r}\left\{\sum_{n=0}^{\infty}\frac{1}{(2\nu t)^{2n}}\left(D_{00}(n,r_o,t)-D_{00}\left(n,0^+,t\right)\right)\cdot\left[\left(D_2(n,b,r,z,t)-D_2\left(n,b,0^+,z,t\right)\right)-\left(D_2(n,a,r,z,t)-D_2\left(n,a,0^+,z,t\right)\right)\right]\right\} \tag{46}$$

Where the above expression for the incremental radial vorticity incorporates two new functions

$$D_2(n,\alpha,\beta,z,t) \equiv -2\nu t\cdot\sum_{j=0}^{n}\frac{n!(2j-1)!!}{(n-j)!\,j!}D_{20}(j,\alpha,z,t)\beta^{2(n-j)}e^{-\beta^2/4\nu t}\cdot\sum_{k=0}^{n-j}\frac{(n-j)!\left(2\sqrt{\nu t}/\beta\right)^{2k}}{(n-j-k)!}$$

And where

$$D_{20}(j,\alpha,z,t) \equiv \frac{d}{dz}D_{10}(j,\alpha,z,t) \tag{47a-b}$$

Now, given the standard handbook formula

$$\frac{d}{dz}erf(x) = \frac{2}{\sqrt{\pi}}e^{-x^2}\cdot\frac{dx}{dz} \tag{48}$$

And making the indicated substitution, Eq. 35b into Eq. 47b, yields

$$\begin{aligned} D_{20}(j,\alpha,z,t) = {} & 2(2j-1)\nu t(z-\alpha)^{2(j-1)}e^{-(z-\alpha)^2/4\nu t}\cdot\sum_{m=0}^{j-1}\frac{\left(2\sqrt{\nu t}/(z-\alpha)\right)^{2m}}{2^m(2j-2m-1)!!} \\ & -(z-\alpha)^{2j}e^{-(z-\alpha)^2/4\nu t}\cdot\sum_{m=0}^{j-1}\frac{\left(2\sqrt{\nu t}/(z-\alpha)\right)^{2m}}{2^m(2j-2m-1)!!} \\ & -2\nu t(z-\alpha)^{2j-1}e^{-(z-\alpha)^2/4\nu t}\cdot\sum_{m=0}^{j-1}\frac{2m(2\nu t)^m}{(z-\alpha)^{2m+1}(2j-2m-1)!!} \\ & -2^j(\nu t)^j e^{-(z-\alpha)^2/4\nu t} \end{aligned} \tag{49}$$

Note that in the above (and subsequent analysis), the following convention holds: $\sum_{i=n}^{m}x_i = 0$ if $m<n$ and $\sum_{i=n}^{m}x_i = x_n$ if $m=n$.

An intermediate function, $h(\gamma, r_o, a, b, r, z, t)$, leading to the estimation of the azimuthal vorticity will now be derived. Given the axisymmetric definition of the azimuthal vorticity

$$\omega_\theta = \frac{\partial v_r}{\partial z} - \frac{\partial v_z}{\partial r} \tag{50}$$

The above relationship implies the following function definition

$$h = \frac{\partial}{\partial z}(\Delta\omega_r) - \frac{\partial}{\partial r}(\Delta\omega_z) \tag{51}$$

Through "localized" application of length scale factors, and summation of incremental contributions to the azimuthal vorticity, the following result can be established

$$\omega_\theta = \sum \Delta\omega_\theta = \sum_i \ell_i h_i \tag{52}$$

Therefore, the following initial derivative is derived to define the intermediate function $h(\gamma, r_o, a, b, r, z, t)$

$$\frac{\partial}{\partial z}(\Delta\omega_r) = \frac{-3\gamma}{8 r_o^3 \sqrt{\pi^3 \nu t}\cdot r}\left\{\sum_{n=0}^{\infty}\frac{1}{(2\nu t)^{2n}}\left(D_{00}(n, r_o, t) - D_{00}\left(n, 0^+, t\right)\right)\right.$$
$$\left.\cdot\left[\left(D_3(n, b, r, z, t) - D_3\left(n, b, 0^+, z, t\right)\right) - \left(D_3(n, a, r, z, t) - D_3\left(n, a, 0^+, z, t\right)\right)\right]\right\}$$

Where

$$D_3(n, \alpha, \beta, z, t) \equiv \frac{d}{dz} D_2(n, \alpha, \beta, z, t) \tag{53a-b}$$

Or

$$D_3(n, \alpha, \beta, z, t) \equiv -2\nu t \cdot \sum_{j=0}^{n} \frac{n!(2j-1)!!}{(n-j)!\, j!} D_{30}(j, \alpha, z, t)\beta^{2(n-j)} e^{-\beta^2/4\nu t} \cdot \sum_{k=0}^{n-j} \frac{(n-j)!\left(2\sqrt{\nu t}/\beta\right)^{2k}}{(n-j-k)!}$$

With

$$D_{30}(j, \alpha, z, t) \equiv \frac{d}{dz} D_{20}(j, \alpha, z, t) \tag{54a-b}$$

Such that

$$D_{30}(j, \alpha, z, t) = D_{301}(j, \alpha, z, t) + D_{302}(j, \alpha, z, t) + D_{303}(j, \alpha, z, t) + D_{304}(j, \alpha, z, t)$$

With the following

$$D_{301}(j,\alpha,z,t) = 4(j-1)(2j-1)\nu t(z-\alpha)^{2j-3}e^{-(z-\alpha)^2/4\nu t}\cdot\sum_{m=0}^{j-1}\frac{\left(2\sqrt{\nu t}/(z-\alpha)\right)^{2m}}{2^m(2j-2m-1)!!}$$
$$-(2j-1)(z-a)^{2j-1}e^{-(z-\alpha)^2/4\nu t}\cdot\sum_{m=0}^{j-1}\frac{\left(2\sqrt{\nu t}/(z-\alpha)\right)^{2m}}{2^m(2j-2m-1)!!}$$
$$-2(2j-1)\nu t(z-\alpha)^{2(j-1)}e^{-(z-\alpha)^2/4\nu t}\cdot\sum_{m=0}^{j-1}\frac{2m(2\nu t)^m}{(z-\alpha)^{2m+1}(2j-2m-1)!!}$$

$$D_{302}(j,\alpha,z,t) = -2j(z-\alpha)^{2j-1}e^{-(z-\alpha)^2/4\nu t}\cdot\sum_{m=0}^{j-1}\frac{\left(2\sqrt{\nu t}/(z-\alpha)\right)^{2m}}{2^m(2j-2m-1)!!}$$
$$+\frac{1}{2\nu t}(z-\alpha)^{2j+1}e^{-(z-\alpha)^2/4\nu t}\cdot\sum_{m=0}^{j-1}\frac{\left(2\sqrt{\nu t}/(z-\alpha)\right)^{2m}}{2^m(2j-2m-1)!!}$$
$$+(z-\alpha)^{2j}e^{-(z-\alpha)^2/4\nu t}\cdot\sum_{m=0}^{j-1}\frac{2m(2\nu t)^m}{(z-\alpha)^{2m+1}(2j-2m-1)!!}$$

$$D_{303}(j,\alpha,z,t) = -2(2j-1)\nu t(z-\alpha)^{2(j-1)}e^{-(z-\alpha)^2/4\nu t}\cdot\sum_{m=0}^{j-1}\frac{2m(2\nu t)^m}{(z-\alpha)^{2m+1}(2j-2m-1)!!}$$
$$+(z-\alpha)^{2j}e^{-(z-\alpha)^2/4\nu t}\cdot\sum_{m=0}^{j-1}\frac{2m(2\nu t)^m}{(z-\alpha)^{2m+1}(2j-2m-1)!!}$$
$$+2\nu t(z-\alpha)^{2j-1}e^{-(z-\alpha)^2/4\nu t}\cdot\sum_{m=0}^{j-1}\frac{2m(2m+1)(2\nu t)^m}{(z-\alpha)^{2m+2}(2j-2m-1)!!}$$

$$D_{304}(j,\alpha,z,t) = 2^{j-1}(\nu t)^{j-1}(z-\alpha)e^{-(z-\alpha)^2/4\nu t}$$

(55a-d)

Finally, the second derivative contributing to the intermediate function, $h(\gamma,r_o,a,b,r,z,t)$, can be derived as follows

$$\frac{\partial}{\partial r}(\Delta\omega_z) = \frac{3\gamma}{8r_o^3\sqrt{(\pi\nu t)^3}}D_4(r_o,a,b,r,z,t)$$

Where

$$D_4(r_o,a,b,r,z,t) \equiv \frac{d}{dr}D_0(r_o,a,b,r,z,t)$$

Further

$$D_4(r_o,a,b,r,z,t) = D_{40}(r_o,a,b,r,z,t) + D_{41}(r_o,a,b,r,z,t)$$

Where

$$D_{40}(r_o,a,b,r,z,t) = -\frac{r}{2\nu t}\cdot D_0(r_o,a,b,r,z,t)$$

$$D_{41}(r_o,a,b,r,z,t) =$$
$$\nu t e^{-r^2/4\nu t}\cdot\sum_{n=0}^{\infty}\frac{1}{(2\nu t)^{2n}}\left(D_{00}(n,r_o,t)-D_{00}\left(n,0^+,t\right)\right)\left(D_{410}(n,b,r,z,t)-D_{410}(n,a,r,z,t)\right)$$

And

$$D_{410}(n,\alpha,r,z,t) \equiv \frac{d}{dr}D_{01}(n,\alpha,r,z,t)$$

Or

$$D_{410}(n,\alpha,r,z,t) \equiv -\sum_{j=0}^{n}2(n-j)\frac{n!(2j-1)!!}{(n-j)!\,j!}r^{2(n-j)-1}\cdot\left\{\sqrt{\pi}\cdot 2^j(\nu t)^{j+1/2}erf\left(\frac{z-\alpha}{2\sqrt{\nu t}}\right)\right.$$
$$\left.-2\nu t(z-\alpha)^{2j-1}e^{-(z-\alpha)^2/4\nu t}\cdot\sum_{m=0}^{j-1}\frac{\left(2\sqrt{\nu t}/(z-\alpha)\right)^{2m}}{2^m(2j-2m-1)!!}\right\}$$

(56a-g)

Which taken altogether gives the following expression for the intermediate function, $h(\gamma,r_o,a,b,r,z,t)$

$$h(\gamma,r_o,a,b,r,z,t) =$$
$$\frac{-3\gamma}{8r_o^3\sqrt{\pi^3\nu t}\cdot r}\left\{\sum_{n=0}^{\infty}\frac{1}{(2\nu t)^{2n}}\left(D_{00}(n,r_o,t)-D_{00}\left(n,0^+,t\right)\right)\right.$$
$$\left.\cdot\left[\left(D_3(n,b,r,z,t)-D_3\left(n,b,0^+,z,t\right)\right)-\left(D_3(n,a,r,z,t)-D_3\left(n,a,0^+,z,t\right)\right)\right]\right\}$$
$$-\frac{3\gamma}{8r_o^3\sqrt{(\pi\nu t)^3}}D_4(r_o,a,b,r,z,t)$$

(57)

This concludes the analytical work related to the use of finite-volume spherical source terms to derive incremental velocity and vorticity expressions for the arbitrary span vortex filament segments.

Expressions relating the spherical finite-volume source radii, r_{oA} and $\eta_A r_{oA}$, to the vortex core radius, r_{c0}, where as defined earlier for the upstream far-field vortex geometry $r_{c0} = r_{c0A}$, will now be derived. The vortex filament reconnection solution documented in the main body of paper poses some unique challenges. First of all, the series solutions derived for the vortex vorticity and velocities appear to be semi-convergent in the sense that the initial vorticity and velocity distributions ($t^\bullet = 0$) cannot be directly estimated. (Depending upon where the series are truncated, and the estimation tolerances used in the numerical algorithms employed, the earliest time demonstrated where an accurate solution has been estimated is $t^\bullet \approx 0.02 - 0.03$ – close but not quite good enough.) An alternate approach to solve for these initial vorticity and velocity distributions needs to be defined. Second, there has not been derived, yet, an explicit relationship/dependence of the finite-volume spherical source radii, r_{oA} and $\eta_A r_{oA}$, (used to define the initial axial vorticity) and the initial tangential velocity profile core radius, r_{c0}. Without such an explicit relationship the proper spatiotemporal scaling of the flow cannot be completed. The following analysis seeks to address both analytical issues.

An alternate approach, examining the asymptotic analytical behavior of the axial vorticity and tangential velocity equations, will now be outlined. Without any loss of generality, for reasons of both simplicity and brevity, the columnar vortex version of Eq. 17 will be used for the subsequent analysis.

$$\begin{aligned}
\omega_z = {} & \frac{3\gamma_A}{8\pi r_{oA}^3}\int_{-\infty}^{\infty} erf\left(\frac{\sqrt{r^2+z_*^2}+r_{oA}}{2\sqrt{\nu t}}\right)dz_* - \frac{3\gamma_A}{8\pi r_{oA}^3}\int_{-\infty}^{\infty} erf\left(\frac{\sqrt{r^2+z_*^2}-r_{oA}}{2\sqrt{\nu t}}\right)dz_* \\
& - \frac{3\gamma_A}{4r_{oA}^3}\sqrt{\frac{\nu t}{\pi^3}}\int_{-\infty}^{\infty}\frac{e^{-\left(\sqrt{r^2+z_*^2}-r_{oA}\right)^2/4\nu t}}{\sqrt{r^2+z_*^2}}dz_* + \frac{3\gamma_A}{4r_{oA}^3}\sqrt{\frac{\nu t}{\pi^3}}\int_{-\infty}^{\infty}\frac{e^{-\left(\sqrt{r^2+z_*^2}+r_{oA}\right)^2/4\nu t}}{\sqrt{r^2+z_*^2}}dz_* \\
& + \frac{3\chi_A\gamma_A}{8\pi\left(\eta_A r_{oA}\right)^3}\int_{-\infty}^{\infty} erf\left(\frac{\sqrt{r^2+z_*^2}+\eta_A r_{oA}}{2\sqrt{\nu t}}\right)dz_* - \frac{3\chi_A\gamma_A}{8\pi\left(\eta_A r_{oA}\right)^3}\int_{-\infty}^{\infty} erf\left(\frac{\sqrt{r^2+z_*^2}-\eta_A r_{oA}}{2\sqrt{\nu t}}\right)dz_* \\
& - \frac{3\chi_A\gamma_A}{4\left(\eta_A r_{oA}\right)^3}\sqrt{\frac{\nu t}{\pi^3}}\int_{-\infty}^{\infty}\frac{e^{-\left(\sqrt{r^2+z_*^2}-\eta_A r_{oA}\right)^2/4\nu t}}{\sqrt{r^2+z_*^2}}dz_* + \frac{3\chi_A\gamma_A}{4\left(\eta_A r_{oA}\right)^3}\sqrt{\frac{\nu t}{\pi^3}}\int_{-\infty}^{\infty}\frac{e^{-\left(\sqrt{r^2+z_*^2}+\eta_A r_{oA}\right)^2/4\nu t}}{\sqrt{r^2+z_*^2}}dz_*
\end{aligned} \tag{58}$$

Given Eq. 58, an asymptotic expression for the axial vorticity function at time equal to zero, $\omega_z\big|_{t\to 0}$ can be defined. In particular, it will be formulated so as to treat the approach to the limit $t \to 0$ as a two-step process (with the inner limit approached first). Further, making the substitution $x \equiv \sqrt{r_{oA}^2 - r^2}$ and $x_1 \equiv \sqrt{\eta_A^2 r_{oA}^2 - r^2}$, Eq. 58 can be reduced to

$$\begin{aligned}
\omega_z\big|_{t\to 0} = {} & \frac{3\gamma_A}{4\pi r_{oA}^3}\int_{-x}^{+x} dz_* + \frac{3\chi_A\gamma_A}{4\pi\left(\eta_A r_{oA}\right)^3}\int_{-x_1}^{+x_1} dz_* \\
& - \frac{3\gamma_A}{4r_{oA}^3}\sqrt{\frac{\nu t}{\pi^3}}\cdot C_1\Big|_{t\to 0} + \frac{3\gamma_A}{4r_{oA}^3}\sqrt{\frac{\nu t}{\pi^3}}\cdot C_2\Big|_{t\to 0} \\
& - \frac{3\chi_A\gamma_A}{4\left(\eta_A r_{oA}\right)^3}\sqrt{\frac{\nu t}{\pi^3}}\cdot C_3\Big|_{t\to 0} + \frac{3\chi_A\gamma_A}{4\left(\eta_A r_{oA}\right)^3}\sqrt{\frac{\nu t}{\pi^3}}\cdot C_4\Big|_{t\to 0}
\end{aligned} \tag{59}$$

Which, completing the integration with respect to z_* and recognizing the implied maximum value of r with respect to r_{oA} and $\eta_A r_{oA}$, gives

$$\omega_z\big|_{t\to 0} = \frac{3\gamma_A}{4r_{oA}^3}\sqrt{\frac{\nu t}{\pi^3}}\cdot\left(C_2 - C_1\right)\Big|_{t\to 0} + \frac{3\gamma_A}{2\pi r_{oA}^3}u\left(r_{oA}^2 - r^2\right)\sqrt{r_{oA}^2 - r^2}$$
$$+\frac{3\chi_A\gamma_A}{4\left(\eta_A r_{oA}\right)^3}\sqrt{\frac{\nu t}{\pi^3}}\cdot\left(C_4 - C_3\right)\Big|_{t\to 0} + \frac{3\chi_A\gamma_A}{2\pi\left(\eta_A r_{oA}\right)^3}u\left(\eta_A^2 r_{oA}^2 - r^2\right)\sqrt{\eta_A^2 r_{oA}^2 - r^2} \tag{60}$$

Note that the above integration constants -- C_1, C_2, C_3, and C_4 -- are constants with respect to z_* and not necessarily with respect to other parameters, i.e. specifically it is anticipated that $C_1 \propto C_2 \propto C_3 \propto C_4 \propto f(t)$. It is assumed that the following constraints apply: $C_2 \neq C_1$, $C_4 \neq C_3$, and $C_4 \propto C_3 \propto C_2 \propto C_1 \propto 1/\sqrt{t}$. From a convenience perspective, let $C_1 = -C_2 = -c_1\sqrt{\pi/\nu t}$ and $C_3 = -C_4 = -c_2\sqrt{\pi/\nu t}$, where c_1 and c_2 are resultant constants that will be derived later. As will be seen, there is no loss of generality by making this substitution. The above equation can now be re-expressed as follows

$$\omega_z\big|_{t\to 0} = \frac{3\gamma_A}{2\pi r_{oA}^3}u\left(r_{oA}^2 - r^2\right)\left(c_1 + \sqrt{r_{oA}^2 - r^2}\right)$$
$$+\frac{3\chi_A\gamma_A}{2\pi\left(\eta_A r_{oA}\right)^3}u\left(\eta_A^2 r_{oA}^2 - r^2\right)\left(c_2 + \sqrt{\eta_A^2 r_{oA}^2 - r^2}\right) \tag{61}$$

Where the resultant constants, c_1 and c_2, will be derived from the tangential velocity constraints and conditions.

Considering next the vortex circulation, γ_∞, which is assumed constant for all flow in the upstream and downstream far-field (i.e. along the semi-infinite segments of the vortex filament), a relationship interrelating the vortex segment circulation strengths can be defined.

$$\gamma_\infty \equiv \Gamma\big|_{\substack{r\to\infty \\ z\to\pm\infty}} \equiv 2\pi\int_0^r \omega_z r dr\Big|_{\substack{r\to\infty \\ z\to\pm\infty}} \tag{62}$$

Or, for the above initial vorticity distribution, the following holds

$$\gamma_\infty = \frac{3\gamma_A}{r_{oA}^3}\cdot\int_0^{r_{oA}} r\left(c_1 + \sqrt{r_{oA}^2 - r^2}\right)dr + \frac{3\chi_A\gamma_A}{\left(\eta_A r_{oA}\right)^3}\cdot\int_0^{\eta_A r_{oA}} r\left(c_2 + \sqrt{\eta_A^2 r_{oA}^2 - r^2}\right)dr$$
$$= \frac{3\gamma_A}{r_{oA}^3}\left\{\frac{c_1}{2}r^2 - \frac{1}{3}\sqrt{\left(r_{oA}^2 - r^2\right)^3}\right\}\Big|_0^{r_{oA}} + \frac{3\chi_A\gamma_A}{\left(\eta_A r_{oA}\right)^3}\left\{\frac{c_2}{2}r^2 - \frac{1}{3}\sqrt{\left(\eta_A^2 r_{oA}^2 - r^2\right)^3}\right\}\Big|_0^{\eta_A r_{oA}} \tag{63}$$

Additionally

$$\chi_A \gamma_A = \frac{3\chi_A \gamma_A}{\left(\eta_A r_{oA}\right)^3}\left\{\frac{c_2}{2} r^2 - \frac{1}{3}\sqrt{\left(\eta_A^2 r_{oA}^2 - r^2\right)^3}\right\}\Bigg|_0^{\eta_A r_{oA}} \tag{64}$$

Applying the integration limits to Eqs. 63 and 64 and simplifying yields

$$\frac{\gamma_\infty}{\gamma_A} = 1 + \frac{3c_1}{2r_{oA}} + \chi_A\left(\frac{3c_2}{2\eta_A r_{oA}} + 1\right)$$

And

$$c_2 = 0 \tag{65a-b}$$

Equation 65a is subject to the constraint that for all η_A, within the range of $0 \le \eta_A \le 1$, if $\chi_A = 0$ then $\gamma_\infty / \gamma_A = 1$. Therefore, the following holds

$$c_1 = -\frac{\chi_A}{\eta_A} c_2 \tag{66}$$

And so, given Eq. 65b, therefore

$$\frac{\gamma_\infty}{\gamma_A} = 1 + \chi_A \tag{67}$$

An ordinary differential equation can be defined for the tangential velocity in terms of the axial vorticity.

$$\omega_z = \frac{\partial v_\theta}{\partial r} + \frac{v_\theta}{r}$$

Or

$$\frac{d v_\theta|_{t\to 0}}{dr} + P(r) v_\theta|_{t\to 0} = Q(r) \tag{68a-b}$$

Where

$$P(r) = 1/r$$

And

$$Q(r) = \frac{3\gamma_A}{2\pi r_{oA}^3} u\left(r_{oA}^2 - r^2\right)\left(c_1 + \sqrt{r_{oA}^2 - r^2}\right) + \frac{3\chi_A \gamma_A}{2\pi\left(\eta_A r_{oA}\right)^3} u\left(\eta_A^2 r_{oA}^2 - r^2\right)\left(c_2 + \sqrt{\eta_A^2 r_{oA}^2 - r^2}\right) \tag{68c-d}$$

Which has the general solution

$$v_\theta\big|_{t\to 0} = \left\{ \int Q(r) e^{\int P(r)dr} dr + C \right\} e^{-\int P(r)dr}$$

Where, recognizing the piecewise nature of the resulting tangential velocity profile

$$v_\theta\big|_{\substack{t\to 0 \\ r<\eta_A r_{oA}}} = \frac{1}{r}\left\{ \frac{3\gamma_A}{2\pi r_{oA}^3}\left(\frac{1}{2}c_1 r^2 - \frac{1}{3}\sqrt{\left(r_{oA}^2 - r^2\right)^3} \right) + \frac{3\chi_A\gamma_A}{2\pi\left(\eta_A r_{oA}\right)^3}\left(\frac{1}{2}c_2 r^2 - \frac{1}{3}\sqrt{\left(\eta_A^2 r_{oA}^2 - r^2\right)^3} \right) + C \right\}$$

$$v_\theta\big|_{\substack{t\to 0 \\ \eta_A r_{oA}\le r\le r_{oA}}} = \frac{1}{r}\left\{ \frac{3\gamma_A}{2\pi r_{oA}^3}\left(\frac{1}{2}c_1 r^2 - \frac{1}{3}\sqrt{\left(r_{oA}^2 - r^2\right)^3} \right) + C \right\}$$

$$v_\theta\big|_{\substack{t\to 0 \\ r>r_{oA}}} = \frac{1}{r}C$$

(69a-d)

Given the boundary condition $v_\theta\big|_{t\to 0} = 0$ at $r = 0$, then the constant, C, must be given by $C = \left(1+\chi_A\right)\gamma_A / 2\pi$. The initial tangential velocity distribution, therefore, can be expressed as

$$v_\theta\big|_{t\to 0} = \frac{\gamma_A}{2\pi r}\left\{ 1 + \chi_A + \frac{3}{r_{oA}^3}u\left(r_{oA}^2 - r^2\right)\left(\frac{1}{2}c_1 r^2 - \frac{1}{3}\sqrt{\left(r_{oA}^2 - r^2\right)^3} \right) + \frac{3\chi_A}{\left(\eta_A r_{oA}\right)^3}u\left(\eta_A^2 r_{oA}^2 - r^2\right)\left(\frac{1}{2}c_2 r^2 - \frac{1}{3}\sqrt{\left(\eta_A^2 r_{oA}^2 - r^2\right)^3} \right) \right\}$$

(70)

The constraint is now imposed that there are no velocity jumps at $r = r_{oA}$. Therefore, given this constraint and Eq. 69c-d, then $c_1 = 0$, which is consistent with previous results.

Differentiating the above expression in terms of the radial coordinate and noting that peak tangential velocity occurs when $dv_\theta / dr = 0$, then an expression for the initial vortex core size, r_{c0A}, in terms of the finite-volume spherical source radius, r_{oA}, can be derived. Noting that, for most cases, r_{c0A} lies somewhere within the range $\eta_A r_{oA} \le r_{c0A} \le r_{oA}$, then the following holds

$$\left.\frac{dv_\theta\big|_{t\to 0}}{dr}\right|_{r=r_{c0A}} = \frac{-\gamma_A}{2\pi r_{c0A}^2}\left\{ 1 + \chi_A + \frac{3}{r_{oA}^3}\left(\frac{1}{2}c_1 r_{c0A}^2 - \frac{1}{3}\sqrt{\left(r_{oA}^2 - r_{c0A}^2\right)^3} \right) \right\} + \frac{\gamma_A}{2\pi r_{c0A}}\left\{ \frac{3}{r_{oA}^3}\left(c_1 r_{c0A} + r_{c0A}\sqrt{r_{oA}^2 - r_{c0A}^2} \right) \right\} = 0$$

(71)

Or, substituting for c_1 and simplifying, gives

$$\left(1+\chi_A\right)r_{oA}^3-\sqrt{\left(r_{oA}^2-r_{c0A}^2\right)^3}-3r_{c0A}^2\sqrt{r_{oA}^2-r_{c0A}^2}=0 \tag{72}$$

Equation 72 can be solved numerically yielding the approximate result for the range $-1\le\chi_A<0.4$

$$r_{oA}\approx\left(1+0.075u\left(1+\chi_A\right)\left(1+\chi_A\right)^3\right)r_{c0A} \tag{73}$$

For the special case of $\chi_A=0$, the above expression yields $r_{oA}\approx1.075r_{c0A}$, which is the parabolic core result of Ref. 10. This result also substantiates why, for $\chi_A<<0$, the "dual-core" vortex model presented in Ref. 10 and 11 could successfully employ the artifice that $r_{oA}=r_{c0A}$ in its formulation and solution, even though its source term vorticity distribution deviates significantly from that of a finite volume spherical source (on which it was originally based, at very small values of time) and, therefore, despite r_{oA} being a somewhat meaningless parameter in its original context. Note that there is a singularity at $\chi_A\to0.4$ for Eq. 72; the approximate expression, Eq. 73, does not capture this singularity. In short, Eq. 72 is not valid for specifying the interrelationship between r_{oA} and r_{c0A} if values of $\chi_A\ge0.4$ are used.

Given the above work describing the initial vorticity and velocity distributions, the condition for negative vorticity in the inner core of the vortex is given by the inequality relationship

$$\omega_z\Big|_{\substack{t\to0\\r=0}}\le0 \tag{74}$$

Therefore, negative vorticity in the inner core of the vortex filament will be manifested, for some nonzero period of time, if the following condition is met.

$$\chi_A\le-\eta_A^2 \tag{75}$$

However, as a practical matter, it is also important to define a limit between χ_A and η_A that prohibits the inner core swirling flow to dominate the outer core flow. This can be established by the two equations

$$\max\left(\left|v_\theta\right|\right)\Big|_{\substack{r\le\eta_A r_{oA}\\r=r_{\lim}}}\le\max\left(\left|v_\theta\right|\right)\Big|_{\substack{\eta_A r_{oA}<r\le r_{oA}\\r=r_{c0A}}}$$

$$\left.\frac{\partial v_\theta}{\partial r}\right|_{\substack{t\to0\\r=r_{\lim}}}=0 \tag{76a-b}$$

The result is a set of two nonlinear equations that need to be simultaneously solved for numerically. An approximate solution is given by

$$\chi_A\ge-\left(1.02+\eta_A^3\right)\eta_A \tag{77}$$

The wave front boundary, z_w, will now be derived. The wave front boundary is a somewhat idealized, but essential, flow feature for the vortex reconnection problem. As the initial conditions for the vortex reconnection flow problem include only distributions of nonzero axial vorticity where, further, intentionally so, the radial and azimuthal vorticity is initially zero. The subsequent manifestation ($t > 0$) of nonzero radial and azimuthal vorticity in the flow field can only be the result of creation of vorticity at the wave front boundaries due to the discontinuity, or even steep gradients in the non-ideal sense, of the axial flow, with respect to the axial coordinate, at the boundary. No moving boundary, no continuous creation of radial and azimuthal vorticity, as per the Lagrange theorem regarding vorticity remaining at zero throughout the flow field, if initially at zero, without surfaces/boundaries to create vorticity, e.g. Ref. 16. Consequently, without the wave front boundary, there could not, ultimately, be cross-cancellation of the convective acceleration and vortex-stretching terms in the axial vorticity Helmholtz equation. Therefore, the wave front boundaries are not unnecessary, mathematical only, artifices; their existence is essential. However, the exact nature of the wave front boundaries, and their propagation speed, is difficult to precisely define.

As presented in Ref. 10 and 11, the wave front boundary is assumed to be a function of time and the axial coordinate; therefore the boundary could be analogously thought of as a complementary set of two plane waves (for two breakpoints in close proximity to each other) traveling outward from the initial vortex filament breakpoints. The approximate expression for the wave front propagation velocity, v_p, as originally employed in Refs. 10-11, is

$$v_p \approx \frac{2}{r_{c0}^2} \int_0^\infty v_z\big|_{Free} r dr \Bigg|_{z \to \infty} \tag{78}$$

Which yielded, in turn, for the dual-core vortex model, and by extension the other vortex core models, the result that the wave front propagation velocity was approximately constant, thereby simplifying the definition of the boundary location in the velocity and vorticity expressions. This expression, based on the vortex far-field condition and assuming a single cut (two breakpoints), is

$$v_p \approx \left| \frac{\gamma}{\pi r_{c0}} \right| \tag{79}$$

The resulting planar-wave-like wave front boundary – for a "wave front" propagating away from each breakpoint for each vortex filament segment -- is then given by the expression

$$z_w \approx |C| + \left| \frac{\gamma_i}{\pi r_{c0_i}} \right| t \qquad \begin{array}{l} \text{If } a_i \geq 0 \text{ then } C = a_i \\ \text{If } a_i < 0 \text{ then } C = b_i \end{array} \tag{80}$$

Where r_{c0_i} can be derived by inverting Eq. 72, or Eq. 73, to solve for the local vortex core size; e.g.

$$r_{c0_i} \approx \frac{r_{o_i}}{1 + 0.075u\left(1 + \chi_{A_i}\right)\left(1 + \chi_{A_i}\right)^3} \tag{81}$$

Where $\chi_{A_i} = \gamma_i / \gamma_A$, if $\gamma_i / \gamma_A \neq 1$, and $\chi_{A_i} = 0$ for $\gamma_i / \gamma_A = 1$.

Though the conceptual simplicity of the above result is gratifying, it suffers from a number of limitations. First of all, the definition's requirement that $|z| \to \infty$ implies that $t >> 0$. Indeed, though the wave front propagation velocity does asymptotically approach a constant speed, at very small values of time the propagation velocity is not constant. Consequently, at very small values of time, the wave front boundary is over-predicted if constant wave front propagation speed is assumed. Second, the above definition of the wave front propagation speed, suffers from trying to arrive at an equivalent "slug flow" velocity, i.e. $v_z\big|_{equiv} = constant$ for $r \le r_{c0}$ and $v_z\big|_{equiv} = 0$ when $r > r_{c0}$. Third, for vortex filament segments with positive circulation strength, the wave front propagation velocity is equivalent to this quasi-slug-flow velocity. For vortex segments (or inner vortex cores with negative axial vorticity) with negative circulation strength this analogy breaks down. In actuality, the wave front boundary, in this case, does not propagate (necessarily) along with the axial flow but instead progresses with the advancing localized region(s) where there is formation/creation of nonzero radial and azimuthal vorticity (which is initially assumed zero). Case in point, with negative circulation strength, the axial flow is in fact in the opposite direction of the wave front boundary propagation.) Nonetheless, even for this case, the absolute value of the propagation rate is assumed to be equal to that given by Eq. 79.